



<https://theses.gla.ac.uk/>

Theses Digitisation:

<https://www.gla.ac.uk/myglasgow/research/enlighten/theses/digitisation/>

This is a digitised version of the original print thesis.

Copyright and moral rights for this work are retained by the author

A copy can be downloaded for personal non-commercial research or study, without prior permission or charge

This work cannot be reproduced or quoted extensively from without first obtaining permission in writing from the author

The content must not be changed in any way or sold commercially in any format or medium without the formal permission of the author

When referring to this work, full bibliographic details including the author, title, awarding institution and date of the thesis must be given

Enlighten: Theses

<https://theses.gla.ac.uk/>
research-enlighten@glasgow.ac.uk

ProQuest Number: 10647092

All rights reserved

INFORMATION TO ALL USERS

The quality of this reproduction is dependent upon the quality of the copy submitted.

In the unlikely event that the author did not send a complete manuscript and there are missing pages, these will be noted. Also, if material had to be removed, a note will indicate the deletion.



ProQuest 10647092

Published by ProQuest LLC (2017). Copyright of the Dissertation is held by the Author.

All rights reserved.

This work is protected against unauthorized copying under Title 17, United States Code
Microform Edition © ProQuest LLC.

ProQuest LLC.
789 East Eisenhower Parkway
P.O. Box 1346
Ann Arbor, MI 48106 – 1346

AN EMPIRICAL CORRECTION TO LIFTING-SURFACE
THEORIES FOR USE IN TRANSONIC
AEROELASTIC ANALYSES

by

D.B. McIver, B.Sc.(Eng.).

Summary

In this paper, means are investigated whereby the effects on loading of the shock-wave patterns and non-linearities associated with transonic flow may be included in an aeroelastic analysis. These effects if present on a rigid wing would also exist, although in a modified form, for a flexible wing of the same planform under the same flight conditions.

Three methods are described for adjusting linearised theoretical aerodynamic influence coefficients so that the predicted aerodynamic load distribution on a rigid wing at incidence and at the required Mach number agrees with the measured distribution. Thereafter, it is assumed that these modified influence coefficients, which are possibly dependent on incidence, may be applied to the prediction of the load distribution on the same wing planform at the same Mach number but with an arbitrary spanwise twist variation. It is proposed that the methods be applicable throughout the entire speed range but are pursued in detail only for transonic speeds for which the linearised theory break down.

Two methods are tested by applying them to wind-tunnel data

measured at Mach numbers of 0.80 and 0.94 for a series of flexible wings with different geometrical spanwise twist distributions. The elastic twist distribution for each wing under aerodynamic loading is known or can be calculated. The wings are of aspect ratio 4, quarter-chord sweep of 45° and taper ratio of 0.15. Modified influence coefficients are derived from the data for one spanwise twist distribution and are used to predict the pressure distributions for the other twist variations. Good agreement with the measured pressures at selected points is obtained.

Because of the limitation of lifting-surface theories to continuous chordwise and spanwise wing slope distributions, a control surface must normally be replaced by an equivalent continuous slope distribution. The third method of correction is shown to yield an experimental equivalent slope distribution which is compared with the theoretical values.

A theoretical investigation is made of the application of the aerodynamic corrections to the static aeroelastic analysis of a wing with a control, but no numerical solutions are attempted. Comments are given on the extension of the procedure to other planforms and to the case of oscillatory motion.

Memorandum

This research on "Transonic aeroelastic analyses" has been sponsored by the British Aircraft Corporation , and was carried out from October, 1961 to October, 1962 at the University of Glasgow under the supervision of Doctor A.W. Babister. The thesis is submitted for the Degree of Master of Science in the Faculty of Engineering of the University of Glasgow, and it has not previously been submitted, in part or in whole, for a degree or diploma of any other University or examining body. All the work described herein, except where stated otherwise, is that of the author.

UNIVERSITY OF GLASGOW

Department of Aeronautical Engineering

TRANSONIC AEROELASTIC ANALYSES

by

D.B. McIver, B.Sc.

A thesis submitted for the Degree of Master of
Science in the Faculty of Engineering of the University
of Glasgow.

August, 1965.

Contents.

	<u>Page</u>
Summary.	i
Notation.	ii
Chapter 1. Introduction.	1
§1.1 Purpose of research.	1
§1.2 Transonic flow patterns.	2
§1.3 Related research.	7
Chapter 2. Semi-Empirical Corrections to Linear Lifting Surface Theories.	11
§2.1 Derivation of the aerodynamic corrections.	12
§2.1.1 Method I (Point Theory).	14
§2.1.2 Method II.	16
§2.1.3 Method III.	18
§2.2 Control surfaces.	19
Chapter 3. Results.	22
§3.1 The models.	22
§3.2 The "rigid" wing theoretical and experimental pressure distributions.	24
§3.3 Corrected aerodynamic loadings.	25
§3.4 Control surface loading distributions.	27
Chapter 4. The Static Aeroelastic Equations.	29
§4.1 Analysis.	30
Chapter 5. General Discussion and Conclusions.	35
§5.1 Evaluation of method.	35
§5.2 Extensions.	41

Contents (cont.)

	<u>Page</u>
Acknowledgements.	43
References.	44
Appendix.	48
Figures 1 to 14.	

Summary.

Means are investigated whereby the effects on loading of the shock wave patterns and non-linearities associated with transonic flow may be included in a static aeroelastic analysis.

Three methods are described for adjusting linearised theoretical aerodynamic influence coefficients to fit rigid wing measured pressure distributions. The research consists of investigating how well these modified influence coefficients can predict the loading on the same wing at the same Mach number but with an arbitrary spanwise twist distribution.

Two methods are tested by applying them to wind-tunnel data measured at Mach numbers of 0.80 and 0.94 for a series of twisted wings. The wings are of aspect ratio 4, quarter-chord sweep of 45° and taper ratio of 0.15. Good agreement of the modified theory with the measured pressures at selected points on the wings is obtained, especially for high incidences.

The third method, although not pursued in detail, is shown to provide a control surface equivalent slope distribution which is compared with the theoretical values. This may be of use in flutter calculations.

Further research which is required is mentioned and the extension of the method to oscillatory aerodynamics is discussed briefly.

Notation.

$\alpha_j = w_j/V$	wing mean camber-line slope at the point $(x, y)_j$.
A_{ij}	aerodynamic influence coefficient.
$a_{i0}, a_{i1}, a_{i2}, a_{i3}$	see Equations (2.6) and (2.7).
b_{i1}, b_{i2}, b_{i3}	" " (2.18).
c_{i1}, c_{i2}, c_{i3}	" " (2.26).
G_{ii}	correction factor for the load component P_i .
K_{jj}	" " " " wing slope α_j .
$C_n = \int_0^1 \Delta C_p d(\frac{x}{c})$	wing section normal-force coefficient.
$C_m = \int_0^1 \Delta C_p (\frac{1}{4} - \frac{x}{c}) d(\frac{x}{c})$	" " pitching moment " about the quarter-chord.
$\Delta C_p = (P_e - P_u) / \frac{1}{2} \rho V^2$	pressure coefficient.
$\frac{1}{2} \rho V^2$	free-stream dynamic pressure.
M	free-stream Mach number.
P_i	load component at the load point $(x, y)_i$.
R	Reynolds number based on the wing mean chord \bar{c} .
s	wing semispan.
w_j	downwash at the downwash point $(x, y)_j$.
x, y, z	rectangular co-ordinate system attached to the wing, origin at the vertex.
x	positive rearwards.
y	" to starboard.
z	" downwards.
θ_{ij}	structural twist influence coefficient.

Notation (cont.)

Suffices.

E	denotes an experimental or corrected quantity.
T	" a theoretical quantity.
R	" a quantity pertaining to the rigid wing.
F,f	" " " " " " flexible wing.
S	" an elastic structural contribution.
c	continuous component.
d	discontinuous component.

Matrix convention.

[]	square matrix.
[]	diagonal matrix.
{ }	column vector.
[] ⁻¹	matrix inverse.
[I]	unit matrix.

Chapter 1.

Introduction.

§1.1 Purpose of research.

It is well established that the shock wave patterns and flow separation associated with transonic speeds can alter significantly the load distribution and hence the structural deformation of a flexible wing. In many instances these aerodynamic effects may be highly non-linear in character.

The aeroelastician must be able to calculate the aerodynamic load distribution over an arbitrarily cambered wing. At present, he has at his disposal only linearised theories in which, to make the problem more amenable to treatment, inviscid flow is assumed throughout the entire speed range. No simple general theoretical method yet exists whereby viscous and wing thickness effects may be assessed. Consequently, there is much to commend a semi-empirical method that is a synthesis of systematic experiment and a reliable theory. Experiment may serve to correct for the idealisations of theory, which in turn may cater for the parameters that are restricted in wind-tunnel testing.

The development of any aircraft usually necessitates extensive wind-tunnel testing early in its design. Often this will include the measurement of pressure distributions for various Mach numbers and angles of incidence on a nominally rigid wing. It is fitting that these data which, in the past, have generally only been used by the aeroelastician as a comparison for linear

theory, be incorporated in the aeroelastic analysis of the flexible wing.

This report is a modification to and an extension of such a procedure proposed by Gainer (Ref. 1) for wings in supersonic flow. The method is applicable to the complete speed range but is pursued here in detail only for the transonic range for which the linearised theories break down.

Of the many subsonic lifting surface theories available, Richardson's theory is employed to illustrate the methods of correction. A wing (Fig. 1) similar to that dealt with by Gainer is treated and only spanwise twist modes are considered since chordwise deformation is relatively unimportant in moderate and high aspect ratio wings.

§1.2 Transonic flow patterns.

Before proceeding, it will be instructive to consider the limitations of the linearising assumptions. They are valid if

- (i) separation effects are absent, although separation effects which are confined to small areas of the wing can be tolerated (e.g., short bubbles on unswept wings; tip separation on swept wings).
- (ii) angles of incidence, camber and thickness/chord ratios are small. At subsonic speeds there is also the restriction that the camber surface must be continuous otherwise separation will take place. Similar effects occur if the wing leading edge is sharp.

(iii) no regions of mixed subsonic/supersonic flow exist with associated local shocks.

At transonic speeds we are principally concerned with the inability of theory to predict the existence of the complicated shock patterns and regions of separated flow over a wing with their accompanying rapid changes in load distribution.

The phenomena of the formation of the flow about a swept wing-fuselage near Mach 1 is described by Rogers and Hall (Ref. 2) and is related, in the account given below, to the flow about the wing-fuselage considered in this report (Fig. 1). The wing has a known spanwise twist distribution (see Chapter 3 and Figs. 3a-3c) and the flow about it, although not precisely that for the flat wing, will have the same characteristics. In Figures 4a-4c, comparison is made of the theoretical and experimental pressure coefficient distributions. Detailed upper and lower surface pressure distributions may be found in Ref. 12. The wing section has a rounded leading edge.

The initial tip shock.

At low incidences in the subsonic range, flow velocities over the wing are highest near the tip and with a sufficient increase in the free-stream Mach number, which will depend on incidence and wing thickness, a weak tip shock normal to the free-stream is formed. Its inboard extent is small but increases slightly and moves rearwards as the Mach number is increased. The effect of the tip shock on the pressure distribution is small

and is not evident in Figure 4a. It will not be very important aeroelastically for this wing.

The rear shock.

Tip shock development on the upper surface is arrested by the presence of the rear shock which is generally formed at about the same time. Its origin lies in the increase in flow velocity due to the wing thickness. The chordwise increase is greater than the spanwise and consequently the resultant velocity vector is inclined inboard. However, at the wing root, in order to preserve the spanwise symmetry, the flow is constrained to follow the wing or fuselage centre-line. The compression system required to achieve this propagates across the wing span and ultimately coalesces at the tip to form a shock wave of finite strength whose sweep is initially somewhat less than that of the wing leading edge.

In the early stages, the rear shock may propagate into the supersonic flow ahead of the initial tip shock and since, with increase in free-stream Mach number, the former moves rearward more rapidly than the latter, the tip shock is overtaken and disappears. This aft movement of the rear shock is accompanied by an increase in its inboard extent and an associated steepening of the chordwise pressure gradient near the trailing edge farther inboard still. Ultimately, with increase in the free-stream Mach number, the rear shock reaches the wing trailing edge and serves to return the local flow to near the free-stream pressure and direction. Its position changes only slightly with

change in incidence.

The rear shock has a profound effect on the wing load distribution; the pressure on the upper surface aft of the shock increases whereas the pressure coefficient, or in other words the loading experienced by the wing, decreases. Consequently, there is a forward movement of the centre-of-pressure which will affect the elastic twist. In Figure 4b, for a Mach number of 0.80, the rear shock is evident for a root incidence, α_0 , of 8° . Previous to its formation the chordwise pressure coefficient distribution is typically subsonic (Fig. 4a) with a leading edge peak and falling smoothly to zero at the trailing edge. In this case, unlike when the rear shock is present, comparison with theory is reasonable. The higher the Mach number, the lower is the wing incidence at which the rear shock first occurs and in Figure 4a it exists for $M=0.94$ at $\alpha_0=4^\circ$. Agreement with theory is seen to be poor.

Flow separation.

Meanwhile, as incidence increases and the rear shock develops, the flow velocities along the leading edge rise along the entire span. The most rapid changes occur near the tip and the resulting intense pressure gradients lead ultimately to flow separation which starts at the tip and moves progressively inboard with increasing incidence (Figs. 4b and 4c). Separation reduces the local section lift coefficient and moves the centre-of-pressure aft. The chordwise pressure coefficient distribution is characteristically trapezoidal in form with a finite

loading at the trailing edge.

The preceding account covers the main details of the flow for the experimental data used in this report. However, for completeness, we shall continue to explain very briefly the subsequent flow development as the Mach number increases.

The forward shock.

At a higher Mach number, which will depend upon the wing geometry, separation along the leading edge ceases and the flow remains attached to the wing surface as far back as a forward shock which appears to originate close to the wing-fuselage junction and sweeps back outboard over the wing. Flow separation may still occur aft of the shock. This transition from separated to attached leading edge flow is called the transonic flow attachment. The forward shock is not necessarily connected with the attachment process, but arises from the local leading edge conditions and can thus appear at incidences well below that at which leading edge separation takes place.

The outboard, bow and tip shocks.

It is possible for the rear and forward shocks to intersect on the wing surface; the shock between this intersection and the wing tip is called the outboard shock. The pressure rise through this shock is very large and almost inevitably separation takes place. When the stream Mach number reaches unity the bow shock wave forms ahead of the wing. At low and moderate supersonic speeds this exerts only a small influence on the flow over

the wing surface. A further shock which arises to complicate the flow is the tip shock - distinct from the initial tip shock - which is a disturbance within the local supersonic flow, associated with and originating close to the tip leading edge and which indicates the inboard limit of the wing surface influenced by the tip. This shock is comparatively weak but increases in strength with incidence and Mach number.

The above explanation of the transonic flow phenomena is by no means complete but is given merely as an indication of the difficulties involved. It is clear that linearised theory alone falls far short of being able to treat the transonic regime successfully.

§1.3 Related research.

There are many theories which employ experimental two-dimensional results or apply two-dimensional corrections to lifting line and vortex lattice theory (Refs. 3 and 4), but Gainer's paper (Ref. 1) is the only one known to the author which proposes a correction to lifting surface theory from available three-dimensional experimental results. Two-dimensional corrections are unable to cater for the change in loading produced by the shock patterns since they are essentially three-dimensional phenomena.

Gainer derived a method to improve the theoretical pressure distributions for thick wings in supersonic flow. He realised that a thick wing with a detached leading edge shock wave has

certain things in common with a wing having a subsonic leading edge. The flow behind the shock wave is subsonic for some distance and the chordwise pressure distribution has the characteristic leading edge peak. He was able to define a hypothetical "equivalent" wing with a greater sweep angle. This replaced the actual wing with the supersonic leading edge by a wing with a subsonic leading edge and improved the correlation between theory and experiment. When the leading edge of the wing is subsonic, as it is at transonic speeds, the equivalent wing is the same as the actual wing.

Treating this equivalent wing, Gainer then combined the supersonic linearised theory for a wing with a subsonic leading edge with empirical adjustments to give accurate estimates of the steady-state load distributions on an arbitrarily twisted wing over a wide range of angles of incidence. The experimental data used are pressure coefficient distributions measured on a flat wing of the desired planform at the desired Mach number and over the desired range of incidence. On comparing the experimentally and theoretically derived perturbation velocity potentials, he found that whether the wing was flat or twisted, theoretical values were in error by roughly the same percentage at small angles of incidence. Consequently, the actual potential, ϕ_E , at a point could be represented by some constant times the theoretical potential, ϕ_T , the constant being mainly dependent on the location of the point and very little dependent upon the source distribution which caused the

potential. Thus,

$$\phi_E(x, y) = K \phi_T(x, y), \quad . . . (1.1)$$

where K is a constant.

Gainer defines a square matrix, $[S_\phi]$, of aerodynamic influence coefficients which yield the theoretical values of velocity potential in terms of the wing slope distribution, $\alpha(x, y)$, at particular points on the wing:

$$\left\{ \frac{4}{V} \phi_T(x, y) \right\} = [S_\phi] \{ \alpha(x, y) \} . \quad . . . (1.2)$$

Equation (1.2) is adjusted as follows to fit the experimental data:

$$\left\{ \frac{4}{V} \phi_E(x, y) \right\} = [K] [S_\phi] \{ \alpha(x, y) \} \quad . . . (1.3)$$

$$= [K] \left\{ \frac{4}{V} \phi_T(x, y) \right\}, \quad . . . (1.4)$$

where the elements of the diagonal matrix, $[K]$, are defined by Equation (1.1).

Equation (1.4) is now easily solved for $[K]$ to give an exact fit to one set of experimental conditions of $\left\{ \frac{4}{V} \phi_E(x, y) \right\}$ and the slope distribution, $\{ \alpha(x, y) \}$. Although there is no proof that the Equation (1.3) can be applied to the calculation of a potential distribution corresponding to an arbitrary twist distribution, Gainer found that it did so for small angles of incidence when $[K]$ was calculated from flat wing data.

For higher incidences, a non-linear correction becomes necessary. The most suitable form for the influence coefficient equation for cambered and twisted wings is then:

$$\left\{ \frac{4}{V} \phi_E(x, y) \right\} = [K'] [S_\phi] \{ \alpha(x, y) \} + [K''] [S_\phi] [\alpha(x, y)] \{ \alpha(x, y) \} . . . (1.5)$$

where the diagonal matrices $[K']$ and $[K'']$ are calculated

to give an exact fit to the flat wing data.

Sinnott (Ref. 5) has devised an empirical procedure whereby he can predict the shock wave position and pressure distribution on the upper surface of a particular class of aerofoil. His method might be extended to finite wings as more experimental data becomes available but it is notoriously difficult to produce reliable information for transonic speeds. Besides, it is likely that the method could only be applied to a flexible wing by lengthy iteration procedures.

Chapter 2.

Semi-Empirical Corrections to Linear Lifting Surface
Theories

Many linearised aerodynamic theories (Refs. 7,8 and 9) have been devised to calculate the load distribution over the surface of an arbitrarily cambered wing. The choice of any particular method will depend on the free-stream Mach number and the aspect ratio of the wing to be considered.

The theories dealt with in this paper are those in which the relationship between the pressure distribution, $\Delta p(x,y)$, and the downwash distribution, $\alpha(x,y)$, - usually in the form of an integral equation - is satisfied at a finite number of points on the lifting surface. This results in a system of simultaneous linear equations which can be expressed in matrix form as:

$$\{P\} = [A]\{\alpha\} . \quad . \quad . \quad . \quad (2.1)$$

The load vector, $\{P\}$, is a column matrix, the elements of which are the load components, $P_1, P_2, P_3, \dots, P_i, \dots, P_p$, where P_i , a function of the pressure, $\Delta p(x,y)$, may be a discrete lifting force or moment at the "load point" $(x,y)_i$. The downwash vector, $\{\alpha\}$, consists of the non-dimensional downwash components, $\alpha_1, \alpha_2, \alpha_3, \dots, \alpha_j, \dots, \alpha_p$, where α_j is the value at the "downwash point" $(x,y)_j$. Physically, α is the local slope of the wing mean camber surface and is derived from the boundary condition of tangential air flow to the lifting surface.

The number of lift and downwash points chosen will depend largely on the geometry of the wing and on the accuracy of the answer required. A detailed account of their choice can be found in the original papers. There are equal numbers, β , of lift and downwash points.

The square matrix, $[A]$, is composed of load influence coefficients, the element A_{ij} being the load at the i th load point induced by a unit slope at the j th downwash point.

In expanded form, the Equation (2.1) appears as follows:

$$\begin{Bmatrix} P_1 \\ P_2 \\ \vdots \\ P_i \\ \vdots \\ P_p \end{Bmatrix} = \begin{bmatrix} A_{11} & A_{12} & \cdots & A_{1j} & \cdots & A_{1p} \\ A_{21} & A_{22} & \cdots & A_{2j} & \cdots & A_{2p} \\ \vdots & \vdots & & \vdots & & \vdots \\ A_{i1} & A_{i2} & \cdots & A_{ij} & \cdots & A_{ip} \\ \vdots & \vdots & & \vdots & & \vdots \\ A_{p1} & A_{p2} & \cdots & A_{pj} & \cdots & A_{pp} \end{bmatrix} \begin{Bmatrix} \alpha_1 \\ \alpha_2 \\ \vdots \\ \alpha_j \\ \vdots \\ \alpha_p \end{Bmatrix} \quad \cdot \cdot \cdot (2.2)$$

Calculations for this paper were made using Richardson's theory (Ref. 8), a brief summary of which is given in the Appendix. The load components, P_i , considered are the local pressure coefficients, $\Delta C_p(x,y)$, at selected points.

§2.1 Derivation of the aerodynamic corrections.

Since the load influence coefficient matrix, $[A]$, could be considered the source of the discrepancy between theory and experiment, it seems logical, as Gainer suggested, to attempt some modification to it to account for real fluid effects.

For a linear system in real flow, the influence coefficient, independent of the downwash distribution, will be denoted by A_{ij} . Where non-linearities occur, if we can think of a non-linear

influence coefficient, the influence coefficient will be denoted by $A_{ij}(\alpha)$.

Let experimental or corrected quantities carry the subscript "E" and theoretical quantities the subscript "T". Detailed experimental pressure distributions will be required for the wing being considered with a known slope distribution at the required Mach number. Quantities pertaining to this wing - usually rigid - will have the subscript "R".

Theory predicts the following loading for the rigid wing:

$$\{P_R\}_T = [A]_T \{\alpha_R\}, \quad \dots \quad (2.3)$$

where $\{P_R\}_T$ is the theoretical load vector, $[A]_T$ is the theoretical linear influence coefficient matrix and $\{\alpha_R\}$ is the wing slope vector.

From the experimental data for the rigid wing we can construct a load vector $\{P_R\}_E$. Now, in whatever manner the experimental loading differs from that given theoretically, it must still satisfy the physical boundary condition of tangential flow to the wing. Consequently, this condition requires the definition of a modified influence coefficient matrix, $[A(\alpha)]_E$, which may, or may not, be dependent on the local downwash, i.e.,

$$\{P_R\}_E = [A(\alpha)]_E \{\alpha_R\}, \quad \dots \quad (2.4)$$

Equation (2.4) has now to be solved for the matrix $[A(\alpha)]_E$. It is impossible to find a unique solution without some simplifying assumptions being made, but it must be borne in mind that simplicity in application of the corrections is of

major importance.

§2.1.1 Method I (Point Theory).

If $[A(\alpha)]_E$ is a diagonal matrix then the elements are given by:

$$A_{ij}(\alpha)_E = \left. \begin{array}{l} (P_{Ri})_E / (\alpha_{Rj}), \quad i=j \\ = 0 \quad \quad \quad \quad \quad i \neq j \end{array} \right\}, \quad \dots (2.5)$$

and will be constant for linear loading.

Physically, this implies that the loading is a point function of the local slope and although by design, the influence coefficients, $A_{ij}(\alpha)_E$, of Equation (2.5) give the correct loading for the rigid wing, intuitively they might be expected to become progressively more and more inaccurate as the slope distribution increasingly differed from that of the rigid wing. In fact, this is not so as will be shown in Chapter 3. This method might give acceptable results for very high supersonic Mach numbers when only a small portion of the wing can affect each point. This is partly the justification for the use of Piston Theory (Ref.10). However, only investigation of the available data can determine whether reliable results are obtainable.

When the loading is non-linear the influence coefficient, $A_{ii}(\alpha)_E$, will depend on the local slope and we must then resort to a curve-fitting technique. In Chapter 3 it is found that for the rigid wing the load at point $(x,y)_i$, with local incidence α_{Ri} , can be represented quite adequately at low angles of incidence, where the loading is linear, by:

$$(P_{Ri}(\alpha))_E = a_{i0} \alpha_{Ri} \quad , \quad . \quad . \quad . \quad (2.6)$$

and for high values by:

$$(P_{Ri}(\alpha))_E = a_{i1} + a_{i2} \alpha_{Ri} + a_{i3} \alpha_{Ri}^2 \quad , \quad . \quad . \quad . \quad (2.7)$$

where a_{i0} , a_{i1} , a_{i2} , a_{i3} , are constants.

In the former case, the loading is assumed to be antisymmetric about the origin, $\alpha_{Ri} = 0$, and in the latter case only large positive angles of incidence are considered. To deal with large negative incidences all that would be required would be to rewrite Equation (2.7) as:

$$(P_{Ri}(\alpha))_E = -a_{i1} + a_{i2} \alpha_{Ri} - a_{i3} \alpha_{Ri}^2 \quad , \quad . \quad . \quad . \quad (2.8)$$

in which the constants are unchanged. We ignore this case since usually we are only interested in the behaviour of the aircraft at large positive, and not negative, incidences.

In general then, the load vector for the rigid wing is:

$$\{P_R\}_E = [a_1] + [a_2] \{\alpha_R\} + [a_3] \{\alpha_R^2\} \quad , \quad . \quad . \quad . \quad (2.9)$$

where the equation appropriate to linear loading, Equation (2.8), is a particular case of Equation (2.9).

In Chapter 3 we shall investigate the applicability of taking the arbitrary mode load vector, $\{P\}_E$, to be:

$$\{P\}_E = [a_1] + [a_2] \{\alpha\} + [a_3] \{\alpha^2\} \quad , \quad . \quad . \quad . \quad (2.10)$$

where $\alpha(x,y)$ is the slope distribution of the arbitrarily twisted wing at incidence.

This method of obtaining influence coefficients which are consistent with experimental data, is about the simplest possible and may be thought of as a surface analogy to the two-dimensional

strip theory used for high aspect ratio wings. It will be shown in Chapter 3 to give good results for a wing of moderate aspect ratio at high angles of incidence for near-sonic Mach numbers.

§2.1.2 Method II.

The next modification attempted is to the theoretical influence coefficient matrix $[A]_T$, i.e.,

$$[A(\alpha)]_E = [G][A]_T, \quad \dots \quad (2.11)$$

where the matrix $[G]$ is square.

Then, for the rigid wing, the experimental load vector is:

$$\{P_R\}_E = [G][A]_T\{\alpha_R\}, \quad \dots \quad (2.12)$$

and so,

$$\{P_R\}_E = [G]\{P_R\}_T. \quad \dots \quad (2.13)$$

As with Equations (2.4) and (2.5), Equation (2.13) can only be solved for matrix $[G]$ if it is a diagonal matrix, i.e.,

$$\left. \begin{aligned} G_{ij} &= (P_{Ri})_E / (P_{Ri})_T, & i=j \\ &= 0 & i \neq j \end{aligned} \right\}, \quad \dots \quad (2.14)$$

Although there is obviously no proof that the corrections can be applied to the calculation of the loading distribution corresponding to an arbitrary wing slope distribution, it seems reasonable, as in the previous section, to assume that where the slope distribution differs only slightly to that from which the correction factors, G_{ii} , were derived, that by applying them to this distribution a close approximation to the experimental loading can be obtained. In Chapter 3 the ratio $(P_{Ri})_E / (P_{Ri})_T$

is shown to be nearly constant for small angles of incidence.

The modified load vector, $\{P\}_E$, for some spanwise twist mode, $\{\alpha\}$, is then:

$$\{P\}_E = [G][A]_T \{\alpha\} \quad , \quad \cdot \cdot \cdot \quad (2.15)$$

$$= [G]\{P\}_T \quad , \quad \cdot \cdot \cdot \quad (2.16)$$

where $\{P\}_T$ is the theoretical load vector for mode $\{\alpha\}$.

Equation (2.16) illustrates the point that although matrix $[G]$ is a correction to the theoretical influence coefficient matrix, the corrected loading for an arbitrary mode can be evolved from knowledge of only the load vectors. Consequently, theories which provide loading distributions and not influence coefficients may be treated by this method.

When expanded, the modified influence coefficient matrix is:

$$[A]_E = \begin{bmatrix} G_{11}A_{11} & G_{11}A_{12} & \cdot \cdot & G_{11}A_{1j} & \cdot \cdot & G_{11}A_{1p} \\ G_{22}A_{21} & G_{22}A_{22} & \cdot \cdot & G_{22}A_{2j} & \cdot \cdot & G_{22}A_{2p} \\ \cdot & \cdot & \cdot & \cdot & \cdot & \cdot \\ G_{ii}A_{i1} & G_{ii}A_{i2} & \cdot \cdot & G_{ii}A_{ij} & \cdot \cdot & G_{ii}A_{ip} \\ \cdot & \cdot & \cdot & \cdot & \cdot & \cdot \\ G_{pp}A_{p1} & G_{pp}A_{p2} & \cdot \cdot & G_{pp}A_{pj} & \cdot \cdot & G_{pp}A_{pp} \end{bmatrix} \quad \cdot \cdot \quad (2.17)$$

and implies that the load component at point $(x, y)_i$ induced by unit downwashes, α , at the points $(x, y)_j$, $j = 1, 2, 3, \dots, p$, must be factored by G_{ii} to correct for real fluid and wing thickness effects. That is, the correction depends not on the inducing point but on the point induced.

In Chapter 3, G_{ii} is shown to vary with the local slope, α_{Ri} , at high incidences and, as in Equation (2.7), a low order polynomial representation can be used:

$$G_{ii}(\alpha) = b_{i1} + b_{i2}\alpha_i + b_{i3}\alpha_i^2, \quad \dots \quad (2.18)$$

where the constant coefficients b_{i1} , b_{i2} , b_{i3} , are obtained by a curve-fitting procedure on $G_{ii}(\alpha_R)$. As in the previous section, only large positive angles of incidence are considered. It is assumed that the local correction factor is a point function of the local slope and consequently can, by interpolation, be applied to any slope distribution, $\alpha(x, y)$.

The modified load vector for mode $\alpha(x, y)$, as a function of the theoretical load vector, is, from Equations (2.16) and (2.18):

$$\{P\}_E = \left[[b_1] + [b_2][\alpha] + [b_3][\alpha^2] \right] \{P\}_T, \quad \dots \quad (2.19)$$

where,

$$\{P\}_T = [A]_T \{\alpha\}, \quad \dots \quad (2.20)$$

Calculations in Chapter 3 show how significant improvements are obtained over theory using the above corrections.

§2.1.3 Method III.

An alternative modification to the theoretical influence coefficient matrix might be to post-multiply the influence coefficient matrix by a correction matrix:

$$[A]_E = [A]_T [K], \quad \dots \quad (2.21)$$

where the rigid wing experimental load vector is:

$$\{P_R\}_E = [A]_T [K] \{\alpha_R\}, \quad \dots \quad (2.22)$$

Hence,

$$[A]_T^{-1} \{P_R\}_E = [K] \{\alpha_R\} = \{\alpha_R\}_E, \quad \dots \quad (2.23)$$

$$\therefore K_{jj} = (\alpha_{Rj})_E / (\alpha_{Rj}) \quad \dots \quad (2.24)$$

The downwash vector, $\{\alpha_R\}_E$, may be thought of as an equivalent slope matrix and represents the physical wing slope distribution, or more precisely, the slopes at the downwash points required to produce the same potential flow loading on the rigid wing as the loading obtained experimentally. Here, the correction may be applied to the downwash vector rather than directly to the load vector.

The corrected load vector, $\{P\}_E$, for mode $\{\alpha\}$ becomes:

$$\{P\}_E - [A]_T [K] \{\alpha\} = [A]_T \{\alpha\}_E \quad . . . (2.25)$$

and for non-linear corrections,

$$\{P\}_E = [A]_T \left[[C_1] + [C_2] [\alpha] + [C_3] [\alpha^2] \right] \{\alpha\} \quad . . . (2.26)$$

Unlike in Equation (2.17), this correction depends upon the inducing point and not on the point induced. It is not pursued in detail and is introduced here only in connection with the treatment of control surfaces which are dealt with in the following section.

§2.2 Control surfaces.

The controls envisaged are of the form of flaps, ailerons, or elevons. Such controls represent chordwise and spanwise discontinuities in the slope distribution of a wing and the functional representation of the associated pressure distributions in subsonic flow involves singularities along the discontinuities (Ref. 11). No such complications generally arise at supersonic free-stream Mach numbers.

Present day subsonic theories strictly can cater only for

continuous downwash distributions since they do not incorporate the appropriate singular loading functions. However, means exist whereby this shortcoming can be partly overcome.

Richardson proposed the use of equivalent slopes (Ref. 18) to replace the true values. These are defined in such a way that the continuous loading functions give the same integrated loadings as do the discontinuous functions, at least for the two-dimensional chordwise and slender wing theories. For n chordwise collocation points the integrated loadings take the form of total chordwise lift, pitching moment, second pitching moment, up to the $(n-1)$ th pitching moment: in the spanwise sense, they are, for a semispan and m collocation stations, the total lift, rolling moment, second rolling moment, and up to the $(m-1)$ th rolling moment.

The theoretical aerodynamic derivatives produced are not entirely satisfactory but until the appropriate control loading functions are included they must suffice. In aeroelastic calculations, matters might be improved somewhat by the methods of this paper, but this must still be demonstrated. Although the modified theoretical pressure distributions cannot agree in detail with experiment since non-typical loading functions are used, there is the assurance that the corrections applied give the correct pressure at the selected load points for the rigid body mode. The deviations from experiment are thus controlled.

It will be interesting later in Chapter 3 to compare the experimental equivalent slopes, $\{\alpha_R\}_E$, of Equation (2.23) with

Richardson's theoretical equivalent slopes.

The practical treatment of controls is discussed further in Chapter 4 where the correction of Method II is applied to the static aeroelastic equations for a flexible wing with a control surface.

Chapter 3.

Results.

It is now necessary to establish just how well the suggestions outlined in Chapter 2 can improve the predicted loading on a flexible wing at incidence.

The present investigation will be confined to near-sonic Mach numbers for swept wings of moderate aspect ratio. Rather than become involved in the lengthy calculations required in an aeroelastic analysis, it was considered a sufficient test of the method to apply it to rigid wings with varying amounts and distributions of spanwise twist. The prediction of wing camber loadings, which are of more importance aeroelastically on low aspect ratio wings, is left to a later report.

§3.1 The models.

References 12 to 16 provided the necessary experimental pressure distributions. They were obtained from tests in the Langley 8-foot transonic tunnel for a Mach number range of 0.8 to 1.2 on the wing-body planform of Figure 1. The wing had 45° sweepback of the quarter-chord line, an aspect ratio of 4, and a taper ratio of 0.15. The wing section was an NACA 65A206, $a=0$ at the root, varying linearly in thickness to an NACA 65A203, $a=0.8$ (modified) at the 50-percent-semispan station, then remained constant to the tip. Flush-mounted pressure pickups were located at six semispan stations on both upper and

lower wing surfaces. These were at the stations $y/s=0.12, 0.25, 0.40, 0.60, 0.80, 0.95$.

Pressure distributions were available for the geometrically untwisted wing and for it with linear, quadratic and cubic spanwise twist distributions. The wings were flexible and consequently had additional twist distributions due to the distortion under the aerodynamic loading. These were provided or could be calculated. Thus, the actual spanwise twist distributions were known under all loading conditions.

Despite this additional twist, for convenience the wings are called respectively:

Planar Wing I	...	Ref.12,
Planar "	II...	Ref.13,
Linear "	...	Ref.14,
Quadratic "	...	Ref.15,
Cubic "	...	Ref.16.

Figures 3a-3c show the total twist distributions - geometric plus elastic - for the Planar Wing I, Linear and Cubic Wings at several values of root incidence and for $M=0.80$ and 0.94 . These are the only cases dealt with in detail. The test Reynolds numbers for the two Mach numbers are 2.62×10^6 and 2.81×10^6 respectively. The root-chord slope, α_o , and the local flexible wing slope, α_f , are quoted where necessary.

Deviations in Mach number in the tunnel test section do not exceed ± 0.010 . The accuracy of the pressure measurements in coefficient form is believed to be less than ± 0.006 and is well

within the accuracy of a graphical representation of pressure distributions. The measured root-chord incidence, α_o , is correct to within $\pm 0.1^\circ$ and the calculated twist, α_t , to $\pm 0.25^\circ$.

§3.2 The "rigid" wing theoretical and experimental pressure distributions.

The wing from which the corrections are obtained - the so-called rigid wing - is the Planar Wing I. The Planar Wing II is also used for low incidence corrections.

Theoretical pressure distributions, calculated using the standard Deuce computer programmes for Richardson's theory (see the Appendix), are compared with the corresponding experimental values in Figures 4a-4c. Collocation at five chordwise points and six spanwise stations was chosen. Only chordwise pressure coefficient distributions (obtained by interpolation) for the two spanwise stations $y/s=0.40$ and 0.80 and the two Mach numbers 0.80 and 0.94 are considered.

The original wings of Refs. 12 to 16 were cambered and an attempt was made to remove this effect by subtracting the pressure coefficients for the Planar Wing I, $\alpha_o=0$, from those of all the other wings over the complete range of incidence. The twist distributions of Figures 3a-3c have had the twist due to this camber loading removed.

In Figures 5a-5d, the modulus of the pressure coefficients, $|\Delta C_p|$, for the Planar Wings I and II are plotted against the modulus of the local wing slope, $|\alpha|$, for particular points on

the wing. Only the plots for three chordwise points are presented although a total of five points is used to predict the improved loading distributions for the Linear and Cubic Wings in §3.3. By the method of least squares, straight lines - $a_0|\alpha|$ for low incidences and $a_1+a_2|\alpha|$ for high values - are fitted through the points plotted. A straight line fit was found to be adequate in this instance.

Moduli of values are taken since data was available for the Planar Wing II at negative values of root-chord incidence. The plots are the basis of the Point Theory outlined in §2.1.1 and demonstrated in §3.3.

In this exercise, the load components, P_i , are the pressure coefficients at selected points on the wing, $(x, y)_i$. Figures 6a-6d show the correction functions,

$$G_{ii} = (\Delta C_{pi})_{RE} / (\Delta C_{pi})_{RT} ,$$

defined in §2.1.2, for the Planar Wings I and II plotted against the local slope, $|\alpha_i|$. The plots suggest that G_{ii} be a constant for low incidences and for high incidences that it be of parabolic form with respect to $|\alpha_i|$.

The pressure coefficient, ΔC_{pi} , and the correction factor, G_{ii} , are assumed to be antisymmetric and symmetric respectively with the local slope, α_i .

§3.3 Corrected aerodynamic loadings.

The theoretical pressure coefficient distributions for the Linear and Cubic Wings over a wide range of root-chord incidence, α_0 , were calculated using Richardson's method, and are presen-

ted for the two Mach numbers 0.80 and 0.94 in Figures 7a-7c, 8a-8c and 9a-9c. They are compared with the experimental values obtained from References 14 and 16. The elastic contributions to the spanwise twist are given in Figures 3b and 3c.

Values predicted by Methods I and II of Chapter 2 are superimposed on Figures 7a to 9c. The Point Theory pressure coefficients of Method I are obtained by reading from Figures 5a-5d the value of ΔC_{p_i} appropriate to the local wing slope, α_{f_i} . This gives the pressure coefficient at specific points on the wing. Method II, as given by Equation (2.16) or (2.19), consists of multiplying the local theoretical pressure coefficient by a correction factor, G_{ii} , which is obtained from Figures 6a-6c for the appropriate local wing slope.

The spanwise running normal-force and pitching moment coefficients about the quarter-chord, C_n and C_m , are plotted against the local slope, α_f , in Figures 11a and 11b for all wings at the stations $y/s=0.40$ and 0.80 . A line is drawn through the Planar Wing I values. The plots are assumed to be antisymmetric about the origin. Theoretical and experimental

C_n and C_m distributions are shown in Figure 12 for the Linear Wing at $M=0.94$ and $\alpha_o = 4^\circ$ and 12° . The pressure coefficients at the lift points can be converted to the local normal-force and pitching moment with the aid of Equations (A.7), (A.11) and (A.12).

§3.4 Control surface loading distributions.

In §2.1.3 it was shown how an experimental equivalent slope distribution could be obtained for a wing with a control. We apply this now to the wing-control configuration of Figure 2 for a Mach number of 0.94.

Reference 19 provides the pressure distributions on the starboard semispan only, produced by a deflection of 14.5° of the starboard control. Spanwise running normal-force and pitching moment coefficients are known for both semispans and so the distortion under loading can be calculated. At the port and starboard tips the twist was found to be -0.16° and -1.09° respectively. The spanwise variation is assumed to vary linearly from the tip values to zero at the wing root.

The pressure distribution for this control angle also included a contribution due to a wing root-chord incidence of $\alpha_0 = 0.2$. This was removed by subtracting $2/3$ of the pressure distribution given in the same report for a wing slope of $\alpha_0 = 0.3$ and zero control deflection. Due to the relative magnitudes of the various wing slope contributions, the wing distortion was assumed for simplicity to be due entirely to the control loadings and not on the aeroelastically induced loadings.

We require to calculate the theoretical aerodynamic influence coefficients for a wing with an asymmetric slope distribution. The computer programme provides those for symmetric and antisymmetric conditions. It can be shown that these are respectively the sum and difference of two matrices as follows:

$$[A]_{sym} = [a] + [b] \quad ,$$

and,

$$[A]_{antisym} = [a] - [b] \quad ,$$

where matrix $[a]$ is the pressures on the starboard wing produced by unit slopes on the starboard wing and $[b]$ gives the pressures on the starboard wing produced by unit slopes on the port wing. By matrix algebra,

$$[a] = \frac{1}{2} [A_{sym} + A_{antisym}] \quad ,$$

and,

$$[b] = \frac{1}{2} [A_{sym} - A_{antisym}] \quad \bullet$$

Hence, the starboard wing experimental load vector, derived from the pressure distributions, is:

$$\begin{aligned} \{P_{stbd}\}_E &= [a]_T \{\alpha_{stbd}\}_E + [b]_T \{\alpha_{port}\}_E \\ &\doteq [a]_T \{\alpha_{stbd}\}_E \end{aligned}$$

where we have neglected the twist on the port semispan since it is very small relative to the slopes on the starboard semispan. Consequently,

$$\{\alpha_{stbd}\}_E \doteq [a]_T^{-1} \{P_{stbd}\}_E \quad .$$

In Figure 13 the theoretical pressure distribution using Richardson's equivalent slopes for the control is compared with the experimental pressure distribution. Figure 14 shows the theoretical and experimental equivalent slopes.

It is stressed here that the above is merely intended as a demonstration of the method. Obviously there are gross assumption involved but nevertheless it is felt that the results give a reasonable indication of what may be obtained with more precise knowledge of control surface pressure distributions.

Chapter 4.

The Static Aeroelastic Equations.

So far, little has been said about the application of the aerodynamic corrections to an aeroelastic analysis. Obviously, to prove their applicability we must investigate the analysis in some detail. Attention will be confined to the method of direct collocation, in which the displacements at a finite number of selected points on the structure are considered as separate parameters and the lumped forces at these points equilibrated. The equations for the continuous wing are thus reduced to a system of simultaneous linear algebraic equations which can be solved by matrix algebra.

Before deriving the aeroelastic equations, a few initial thoughts are presented on the application of the aerodynamic corrections.

We have seen in Chapter 3 that for low incidences the modified aerodynamic influence coefficients are independent of the wing slope distribution. Consequently, the modified matrix can be applied in exactly the same manner as the theoretical influence coefficient matrix. However, problems arise, as we shall see subsequently, whenever non-linear corrections are necessary.

Usually, elastic displacements are of an order smaller in magnitude than the displacements in the applied rigid body modes, say, of incidence, pitch, roll and control deflection.

Thus, it might reasonably be assumed that the aerodynamic loading induced by the structural deformation is merely a linear addition to the possibly non-linear rigid wing loading. In other words, in the aeroelastic analysis, the experimental aerodynamic loadings for the applied rigid-body wing modes could be used in conjunction with the theoretically derived linear loadings for the distortion modes. However, if distortions were large, a complete non-linear analysis would be required.

The deformation of a lifting surface with controls can be expressed as a sum of continuous and discontinuous parts. This is necessary since, by their nature, different corrections must be applied to each component. We have not yet demonstrated that any of the methods of this paper will give satisfactory improvements to predicted control loadings; nevertheless, it is felt that improvements could be obtained if not by the present methods then by some similar simple procedure. The aerodynamic corrections can be obtained from measured pressure distributions for the rigid wing at incidence (continuous) and for the same wing at zero incidence but with the control deflected (discontinuous).

Rather than investigate the application of all three types of correction to the aeroelastic equations for all possible conditions, we will treat a particular case of a wing with a control. Method II will be used.

§4.1 Analysis.

A structural slope influence coefficient matrix is defined by the square matrix $[\theta]$, where the element θ_{ij} is the elastic slope at the structural node $(x,y)_j$ produced by a unit load element at the point $(x,y)_i$. The matrix contains the effect of wing, control and control jack flexibilities and consequently, contains control slope discontinuities. These can be separated in such a way that,

$$[\theta] = [\theta_c] + [\theta_d] \quad , \quad . . . \quad (4.1)$$

where matrix $[\theta_c]$ has an entirely continuous slope distribution and matrix $[\theta_d]$ is essentially discontinuous. In $[\theta_d]$, the slope over the wing is zero and only points appropriate to control structural modes will have non-zero elements.

The flexible wing slope vector can be expressed as a sum of rigid and elastic structural contributions:

$$\{\alpha_F\} = \{\alpha_R\} + \{\alpha_S\} \quad , \quad . . . \quad (4.2)$$

and in terms of continuous and discontinuous components:

$$\{\alpha_F\} = \{\alpha_{rc}\} + \{\alpha_{rd}\} + \{\alpha_{sc}\} + \{\alpha_{sd}\} \quad . . . \quad (4.3)$$

Assuming that, although by themselves non-linear, when taken together the continuous and discontinuous slope loading contributions are linearly additive, then,

$$\{P_F\}_E = [G_c(\alpha_{Fc})][A]_T \{\alpha_{Fc}\} + [G_d(\alpha_{Fd})][A]_T \{\alpha_{Fd}\} \quad , \quad . . . \quad (4.4)$$

where $[G(\alpha)]$ is of the form:

$$[G(\alpha)] = [b_1] + [b_2][\alpha] + [b_3][\alpha^2] \quad , \quad . . . \quad (4.5)$$

as in Equation (2.18).

If distortions are small compared with the rigid body

contributions, then,

$$[G(\alpha_F)] = [G(\alpha_R)] \quad , \quad \cdot \cdot \cdot \quad (4.6)$$

and,

$$\{P_F\}_E = [G_c(\alpha_{rc})][A]_T \{\alpha_{rc} + \alpha_{sc}\} + [G_d(\alpha_{rd})][A]_T \{\alpha_{rd} + \alpha_{sd}\} \quad , \quad \cdot \cdot \cdot \quad (4.7)$$

Now, the elastic distortions in terms of the loadings are:

$$\{\alpha_{sc}\} = [\theta_c] \{P_{rc}\}_E + [\theta_c] \{P_{rd}\}_E - [\theta_c] \{P_F\}_E \quad , \quad \cdot \cdot \cdot \quad (4.8)$$

and similarly,

$$\{\alpha_{sd}\} = [\theta_d] \{P_F\}_E \quad , \quad \cdot \cdot \cdot \quad (4.9)$$

Therefore, substituting these in Equation (4.7),

$$\begin{aligned} \{P_F\}_E &= [G_c(\alpha_{rc})][A]_T \{\alpha_{rc}\} + [G_d(\alpha_{rd})][A]_T \{\alpha_{rd}\} \\ &+ \left[[G_c(\alpha_{rc})][A]_T [\theta_c] + [G_d(\alpha_{rd})][A]_T [\theta_d] \right] \{P_F\}_E \quad , \quad \cdot \cdot \cdot \quad (4.10) \end{aligned}$$

from which:

$$\{P_F\}_E = \left[[I] - [G_c(\alpha_{rc})][A]_T [\theta_c] - [G_d(\alpha_{rd})][A]_T [\theta_d] \right]^{-1} \{P_{rc} + P_{rd}\}_E \quad (4.11)$$

where $\{P_{rc}\}_E$ and $\{P_{rd}\}_E$ are the continuous and discontinuous rigid-body experimental load vectors respectively. The slope distributions, α_{rc} and α_{rd} , are known and so $\{P_F\}_E$ can be calculated.

It was suggested earlier that it may be sufficient to treat the induced distortion loading by linear theory. Equation (4.11) can then be shown to reduce to:

$$\{P_F\}_E = \left[[I] - [A]_T [\theta] \right]^{-1} \{P_{rc} + P_{rd}\}_E \quad , \quad \cdot \cdot \cdot \quad (4.12)$$

$$= \left[[I] - [A]_T [\theta] \right]^{-1} \{P_R\}_E \quad , \quad \cdot \cdot \cdot \quad (4.13)$$

which has the advantage that the difficult part of the calculation, namely the matrix inversion, remains unaltered with different applied rigid-body loading conditions.

At sufficiently low angles of incidence, the correction

matrix, $[G]$, is constant and so:

$$\{P_F\}_E = \left[[I] - [G_c][A]_T[\theta_c] - [G_d][A]_T[\theta_d] \right]^{-1} \{P_{rc} + P_{rd}\}_E \quad (4.14)$$

Unlike with Equation (4.11), the above inversion will remain unaltered by the rigid-body loading condition provided that it be for a low incidence.

When distortions are relatively large, it may be necessary to use the correction matrix:

$$[G(\alpha_F)] = [b_1] + [b_2][\alpha_F] + [b_2][\alpha_F^2] \quad (4.15)$$

$$\cong [b_1] + [b_2][\alpha_R + \alpha_S] + [b_2][\alpha_R^2 + 2\alpha_R\alpha_S] \quad (4.16)$$

where the term in α_S^2 is neglected in comparison to α_R^2 and $2\alpha_R\alpha_S$. Equation (4.4) must now be written as:

$$\{P_F\}_E = [G_c(\alpha_{Fc})][A]_T \{\alpha_{rc} + \alpha_{sc}\} + [G_d(\alpha_{Fd})][A]_T \{\alpha_{rd} + \alpha_{sd}\} \quad (4.17)$$

and is best solved by iteration. By assuming that:

$$\{P_F\}_{E1} \cong \{P_R\}_E \quad (4.18)$$

the first approximations are as follows:

$$\text{and, } \left. \begin{aligned} \{\alpha_{sc}\}_1 &\cong [\theta_c]\{P_R\}_E \\ \{\alpha_{sd}\}_1 &\cong [\theta_d]\{P_R\}_E \end{aligned} \right\} \quad (4.19)$$

On substituting Equations (4.19) into (4.17), the L.H.S. of Equation (4.17) will yield a second approximation, $\{P_F\}_{E2}$, to the flexible wing load vector. Then,

$$\left. \begin{aligned} \{\alpha_{sc}\}_2 &\cong [\theta_c]\{P_F\}_{E2} \\ \{\alpha_{sd}\}_2 &\cong [\theta_d]\{P_F\}_{E2} \end{aligned} \right\} \quad (4.20)$$

and so on.....

The assumption that the continuous and discontinuous slope loading contributions are linearly additive may be unrealistic at times, but to consider the alternative could lead to a :

prohibitive amount of work in deriving the corrections.

Detailed pressure measurements would be required for the wing over a range of incidence with the control angle varied for each value of wing incidence. However, there is nothing to prevent the use of such data, if available, as the rigid-body load vector, $\{P_{rc} + P_{rd}\}_E$, for example in Equation (4.11), but treating the loading induced by the distortion in the above simplified manner.

Chapter 5.

General Discussion and Conclusions.

§5.1 Evaluation of method.

The speed and flexibility of present-day and future aircraft require that many aerodynamic effects, hitherto ignored, must be accounted for in an aeroelastic analysis. However, at present, theory alone is incapable of dealing with such effects and to be of practical use in aeroelastic calculations, any empirical modification to theoretical aerodynamics must be simple and must satisfy existing data.

The methods of this paper, explained in Chapter 2 and similar to those applied by Gainer (Ref.1), are probably the simplest type of correction but even they involve a substantial increase in labour.

Chordwise deformation of the wing in Figure 1 was considered to be negligible and only normal-force and pitching moment twist influence coefficients are provided in the original papers (Refs. 12 to 16). Consequently, although detailed pressure distributions are investigated in this research, it would have been sufficient to have obtained an accurate assessment of chordwise lift and pitching moments in order to calculate the distortion of the wing under loading. However, this is not so for lower aspect ratios for which chordwise bending is important and for which detailed pressure distributions are essential. It may be hoped that a unified method of correction can be developed which could be

applied with confidence throughout the complete aspect ratio range: if not, one must know precisely the limitations of the method. For this reason, detailed pressure distributions are considered herein.

Predicted pressure distributions for the twisted wings.

The measured pressure coefficient distributions for the Linear and Cubic Wings (Figures 7a-7c, 8a-8c, 9a-9c) show the same essential features as those for the Planar Wing (Figures 4a-4c) but modified by the differences in spanwise twist. At the wing tips this difference in twist is of the order of 5° even at low root-chord incidences. The geometric twist accounts for the greatest component.

Although M=0.80 is treated, the Mach number of 0.94 is of main interest since the measured loadings differ more markedly from those predicted theoretically. The discussion of the results will be confined to this case although the remarks made will be seen to apply also to M=0.80.

Low wing incidences. Figure 10 has been drawn to compare the chordwise pressure distributions for the Planar, Linear, and Cubic Wings at $\alpha_0 = 4.0^\circ$ for M=0.94. It is clear that the rear shock occurs at almost the same chordwise position for all three wings except near the tip of the Linear Wing where it lies slightly farther forward than for the other two. This could arise possibly because the Linear Wing slope at this station is negative. However, the variation is small (within 10% of the local chord).

Thus we are led to the conclusion that not only is the position of the rear shock invariant with wing root incidence (see Chapter 1) but also with spanwise twist distribution - a convenient property for the aerodynamic corrections.

Other points to note from Figure 10 are that at $y/s=0.40$, where the Planar and Cubic Wing slopes are nearly equal, the pressure coefficients are nearly equal. Conversely, the smaller slopes of the Linear Wing give rise to correspondingly lower pressures. At the tip, the greater the nose-down twist, the greater is the load shed, i.e. the Linear Wing shows smaller pressures than does the Cubic Wing. Comparison of the theoretical load distributions show that they vary with twist distribution in approximately the same fashion. All these facts combine to suggest that, by trial and error, we may indeed succeed in deriving an aerodynamic correction procedure which could be applied with some degree of confidence.

Figures 8a and 9a show that theory does not agree with experiment but that the corrected values of Method II, although not defining the rapid chordwise changes in loading due to the rear shock, are an improvement on theory. Certainly, there is an improvement in the local lift and pitching moment at the tip where it will be most important. The Point Theory results of Method I give poor predictions for the loading near the tip but at the root the improvement is comparable to that produced by Method II. One important disadvantage of Point Theory is highlighted by Figure 8a, and that is that the predicted

loading takes the sign of the local slope, which in this case is negative and so produces negative instead of positive pressures. It is clear then from this and also Figure 9a that, where a very large twist exists relative to the applied wing incidence, the loadings predicted by Point Theory are unreliable.

The plots of the correction factor, Q , (Figures 6a-6d) show a lot of scatter at low incidences, especially for $y/s=0.80$. There is not a sufficient number, nor an adequate distribution, of points to tell us whether this scatter implies the omission on our part of some important effect. The best that could be done - and there was some justification - was to take the mean. However, the fact remains that we have "smoothed away" the rapid change in loading produced by the rear shock. Obviously, this needs further investigation.

There are several ways in which we can be in error. In calculating the theoretical pressure distributions we employed a 5 chordwise point collocation and subsequently modified the pressures at the lift points only. Although increasing the number of collocation points would not alter substantially the theoretical distributions, it is conceivable that we require to modify the pressures at a larger number of points. The theoretical loading functions presuppose an infinite pressure peak at the leading edge and zero pressure at the trailing edge. Thus, the modified loadings are unable to yield finite pressure at the leading and trailing edges - a loading condition which can occur at transonic speeds.

A more regular pattern of results with less scatter is evident for the plots of pressure coefficient against local slope (Figures 5a-5d), and since we do not get good predictions from Point Theory this implies, not that there are errors or inaccuracies, but that the assumptions of this method are just not valid within the transonic regime for such wings at low incidence. However, the method is not without its uses as we shall see.

High wing incidences. As the root incidence, α_o , increases, the differences in twist distribution remain approximately unchanged (-5° at the tip) but they become relatively less and less significant. So, intuitively, we might expect smaller differences in the loadings.

Tip separation occurs for all three wings at about $\alpha_o = 8^\circ$ and progresses inboard as incidence increases. Figures 5a-5d indicate that the magnitude of the chordwise pressure coefficients depend mainly on spanwise position and are almost independent of local wing slope and Mach number. The chordwise pressure distribution is typically trapezoidal in form. As might be expected, the Point Theory results improve noticeably as α_o increases until, for $\alpha_o = 20^\circ$, the agreement with experiment is remarkable (Figure 9c).

The results of Method II, which proved superior at low incidences, give good agreement with experiment at these higher incidences but in most cases are no better than the Point Theory values. The latter's simplicity could make it of great

use in aeroelastic analyses.

Spanwise normal-force and pitching moment distributions.

It is not altogether surprising that, with the regularity of the pressure plots of Figures 5a-5d, the local spanwise normal-force and pitching moment coefficients, C_n and C_m , for all the wings can be collapsed as in Figures 11a and 11b. The least scatter is obtained for values at the spanwise station $y/s=0.40$ where the slopes for the wings are all nearly equal.

For a wing of this aspect ratio and planform, a sufficiently good approximation to the deformation can be obtained from the loading considered as concentrated at the flexural axis in the form of a lift and pitching moment. Figures 11a and 11b suggest that they may be predicted by a two-dimensional theory knowing the corresponding values over a range of incidence for a wing with known twist distribution.

Figure 12 illustrates how the measured and theoretical spanwise lift distributions agree at low root-chord incidence. At higher incidences, they disagree since the leading edge vortex causes loss of lift at the tip and a peak further inboard. The agreement with the pitching moment is poor. The modified pressures of Figures 8a and 8c give much improved values of lift and pitching moment.

Control surface loadings.

There is in general very poor agreement between the theore-

tical and measured pressure distributions, due, principally, to the form of the loading functions as explained in §2.2. The equivalent slope distributions differ appreciably, especially over the control itself. It remains to be demonstrated that the control loadings can be improved by any of the above methods.

§5.2 Extensions.

Other planforms. So far, in this paper and Gainer's (Ref. 1), wings of moderate aspect ratio with high quarter-chord sweep have been investigated for transonic and supersonic Mach numbers. Subsequent exercises must deal with the low subsonic regime and other classes of wings, especially deltas.

It is possible that the corrections for one wing may be applied to another wing of slightly different planform. If the wings differ substantially in sweep, aspect ratio or thickness/chord ratio, then possibly the aerodynamic similarity rules (Ref.20) may be utilised in some way to enable the corrections for one wing to be applied to another. This facility could be useful in the event of there being no available measured data for the wing being considered.

Provided the rigid wing measured pressure distributions contain the effects of a fuselage (as do those of the present report) or any other bodies such as engine nacelles, tip stores, etc., then their aeroelastic effects can be assessed by these methods.

Cambered wings. As aspect ratio decreases, the camber and camber loadings become more and more important and consequently investigation must be concentrated on these. Only Methods II and III are likely to give improved results over theory since, as was noted in §5.1, the Point Theory distribution will take the sign of the local slope which is unlikely to give reliable results.

Oscillatory motion. The extension to oscillatory motion is difficult to justify since so very few oscillatory pressure distributions have been measured. It is recognised (Ref. 17) that usually the non-linear effects of shock wave and boundary layer interaction and flow separation are markedly reduced during unsteady motion, although at low frequencies these effects are still present but are not so severe.

The matrix equation relating the oscillatory loading to the downwash distribution is:

$$\{P_x + iP_o\} = [A(\nu) + i\nu B(\nu)] \{\alpha + i\nu h\},$$

where $\nu = \omega l/V$ is the frequency parameter (ω = circular frequency, l = typical wing length, V = airspeed), α is the in-phase downwash and νh is the out-of phase downwash.

Provided that suitable oscillatory pressure distributions were available, one could "correct" the oscillatory influence coefficients to fit this data by modifying the in-phase and out-of-phase components separately. However, it is by no means certain that the modified influence coefficients could be

applied to any other mode. This would require very careful investigation.

For low frequencies, the above equation reduces to:

$$\{P_x + iP_0\} = [A + i\gamma B]\{\alpha + i\gamma h\},$$

where the matrices $[A]$ and $[B]$ are independent of frequency. Matrix $[A]$ is the steady aerodynamic influence coefficient matrix which we have been studying throughout this paper. The loading can be split into four components:

- (i) $[A]\{\alpha\}$ in-phase loading due to in-phase downwash,
- (ii) $-\gamma^2[B]\{h\}$ " " " " out-of-phase downwash,
- (iii) $\gamma[B]\{\alpha\}$ out-of-phase loading due to in-phase downwash,
- (iv) $\gamma[A]\{h\}$ " " " " out-of-phase downwash.

Components (i) and (iv) could possibly be corrected by employing the influence coefficient matrix, $[A]_E$, modified from known steady pressure measurements, in place of the theoretical matrix, $[A]$. Method III would yield equivalent slope distributions for $\{\alpha\}$ and the correction factors might be applied to the out-of-phase downwash vector, $\{h\}$. Thus, the remaining two components, (ii) and (iii), could be modified.

Acknowledgements.

The author wishes to thank the British Aircraft Corporation for their sponsorship of this research and for the use of their Deuce computers. His sincere thanks are also extended to Dr. A.W. Babister for his supervision and encouragement.

References.

1. Gainer, P.A., A method of determining aerodynamic influence coefficients from wind-tunnel data for wings at supersonic speeds. NASA TN D-801.
2. Rogers, E.W.E. An introduction to the flow about plane swept-back wings at transonic speeds. and Hall, I.M., Journal of the Royal Aeronautical Society, August, 1960.
3. Diederich, F.W., A simple approximate method for calculating spanwise lift distributions and aerodynamic influence coefficients at subsonic speeds. NACA TN 2751.
4. Gray, W.L. A method for calculating the subsonic steady-state loading on an airplane with and Schenk, K.M., a wing of arbitrary planform and stiffness. NACA TN 3030.
5. Sinnott, C.S., On the prediction of mixed subsonic/supersonic pressure distributions. Journal of the Aerospace Sciences, October, 1960.
6. Diederich, F.W., Divergence of delta and swept surfaces in the transonic and supersonic speed ranges. AGARD Report 42.

7. Multhopp, H., Methods for calculating the lift distribution of wings (subsonic lifting surface theory).
R & M 2884, 1955.
8. Richardson, J.R., A method for calculating the lifting forces on wings (unsteady subsonic and supersonic lifting surface theory).
R & M 3157, 1960.
9. Pines, S., Aerodynamic flutter derivatives for a flexible wing with supersonic and subsonic edges.
Dugundji, J.,
and
Neuringer, J., Journal of the Aeronautical Sciences, Vol. 22, No. 10, October 1955.
10. Ashley, H. Piston theory - a new aerodynamic tool for the aeroelastician.
and
Zartarian, G., Journal of the Aeronautical Sciences, Vol. 23, No. 12, December 1956.
11. Simpson, R.W., An extension of Multhopp's lifting surface theory.
College of Aeronautics Report 132.
12. Fischetti, T.L., Investigation at Mach numbers from 0.80 to 1.43 of pressure and load distributions over a thin 45° sweptback highly tapered wing in combination with basic and indented bodies.
NACA RM L57D29a.

13. Mugler, J.P., Basic pressure measurements at transonic speeds on a thin 45° sweptback highly tapered wing with systematic spanwise twist variation. Untwisted wing.
NASA MEMO 10-20-58L.
14. Mugler, J.P., Basic pressure measurements at transonic speeds on a thin 45° sweptback highly tapered wing with systematic spanwise twist variations. Wing with linear spanwise twist variation.
NASA MEMO 12-28-58L.
15. Mugler, J.P., Basic pressure measurements at transonic speeds on a thin 45° sweptback highly tapered wing with systematic spanwise twist variations. Wing with quadratic spanwise twist variation.
NASA MEMO 2-24-59L.
16. Mugler, J.P., Basic pressure measurements at transonic speeds on a thin 45° sweprback highly tapered wing with systematic spanwise twist variations. Wing with cubic spanwise twist variation.
NASA MEMO 5-12-59L.
17. Tobak, M., Damping in pitch of low aspect ratio wings at subsonic and supersonic speeds.
NACA RM A52L04a.

18. Richardson, J.R., The application of the Multhopp-Garner theory to the calculation of control surface derivatives.
Fairley Aviation Technical Office
Report 135.
19. Heath, A.R.
and
Igoe, A.W., A wind-tunnel investigation of the wing loads due to deflected ailerons on a 45° sweptback wing at transonic speeds.
NACA RM L58E12.
20. Spreiter, J.R., Similarity laws for transonic flow about wings of finite span.
NACA TN 2273.

Appendix.

The relationship between the pressure distribution, $\Delta p(x, y)$, and the downwash distribution, $w(x, y)$, is:

$$\alpha(x_0, y_0) = -\frac{1}{8\pi} \iint_S \frac{l(x, y)}{(y_0 - y)^2} K(x_0 - x, y_0 - y) dx dy . . . (A.1)$$

where,

$$\alpha(x_0, y_0) = w(x_0, y_0) / V , . . . (A.2)$$

$$l(x, y) = \Delta p(x, y) / \frac{1}{2} \rho V^2 , . . . (A.3)$$

and,

$$K(x_0 - x, y_0 - y) = K(X, Y) = 1 + \frac{x_0 - x}{\sqrt{[(x_0 - x)^2 + \beta^2 (y_0 - y)^2]}} . . . (A.4)$$

The kernel function, $K(X, Y)$, is such that $-K(X, Y) / 8\pi Y^2$ is the non-dimensional downwash, $\alpha(x_0, y_0)$, at (x_0, y_0) induced by an incremental load $dx dy$ at (x, y) .

The basis of Richardson's method lies in satisfying the integral equation at a finite number of selected points on the lifting surface. This allows the replacement of the integral equation (which contains the lift and downwash as functions) by a system of simultaneous linear algebraic equations (containing the values of the lift and downwash at the selected points) which can be expressed in matrix form. These lift and downwash points are carefully chosen to ensure the maximum accuracy from an equation of given matrix order.

The following non-dimensional co-ordinates are defined:

$$\left. \begin{aligned} \xi &= (x - x_{\frac{1}{2}c(\eta)}) / \frac{1}{2}c(\eta) , & -1 \leq \xi \leq +1 \\ \eta &= y / s , & -1 \leq \eta \leq +1 \end{aligned} \right\} , . . . (A.5)$$

The variation of lift over the wing is expressed as the double series:

$$l(\xi, \eta) = \frac{1}{c(\eta)} \sum_{n=-\frac{m-1}{2}}^{\frac{m-1}{2}} c(\eta_n) g_n(\eta) \sum_{q=1}^k l(\xi_q, \eta_n) h_q(\xi) \quad . \quad . \quad (A.6)$$

where $l(\xi_q, \eta_n)$ is the value of the pressure differential, $\Delta p / \frac{1}{2} \rho V^2$, at the lift point, (ξ_q, η_n) , and $h_q(\xi)$ and $g_n(\eta)$ are chordwise and spanwise interpolation functions. The chordwise lift distribution, defined by $h_q(\xi)$, is such that a characteristic infinite peak exists at the wing leading edge falling to zero at the trailing edge. The spanwise distribution tends to zero at the wing tips in the manner $\sqrt{(1-\eta^2)}$.

Richardson goes on to define a set of equivalent discrete loads concentrated at the lift points:

$$P_n = H_q G_n \frac{c(\eta_n)}{\bar{c}} l(\xi_q, \eta_n) \quad , \quad . \quad . \quad (A.7)$$

such that:

$$l(\xi, \eta) = \frac{\bar{c}}{c(\eta)} \sum_{n=-\frac{m-1}{2}}^{\frac{m-1}{2}} \sum_1^k P_n \frac{h_q(\xi)}{H_q} \frac{g_n(\eta)}{G_n} \quad , \quad . \quad . \quad (A.8)$$

where,
$$H_q = \frac{1}{2} \int_{-1}^{+1} h_q(\xi) d\xi \quad , \quad . \quad . \quad (A.9)$$

and,
$$G_n = \frac{1}{2} \int_{-1}^{+1} g_n(\eta) d\eta \quad . \quad . \quad (A.10)$$

The only restriction on the use of the discrete lift forces, P_n , is that the downwash distribution must be a continuous function expressible as a polynomial.

The spanwise distributions of lift and pitching moment about the local quarter-chord are, in terms of the equivalent

loads:

$$C_l(\eta) = \frac{\bar{c}}{c(\eta)} \sum_{n=1}^{m-1} \sum_{q=1}^p P_{nq} \frac{g_n(\eta)}{G_n} , \quad \dots \quad (A.11)$$

$$C_m(\eta) = \frac{\bar{c}}{c(\eta)} \sum_{n=1}^{m-1} \sum_{q=1}^p P_{nq} d_q \frac{g_n(\eta)}{G_n} , \quad \dots \quad (A.12)$$

where,

$$d_q = (x_{\frac{1}{2}c} - x_q) / c(\eta) \quad \dots \quad (A.13)$$

In non-dimensional co-ordinates, Equation (A.1) can be written as:

$$\alpha(\xi_r, \eta_v) = -\frac{1}{4\pi s} \int_{-1}^{+1} \frac{c(\eta)}{(\eta - \eta_v)^2} \int_{-1}^{+1} \ell(\xi, \eta) K\{(x_r - x), (y_v - y)\} d\xi d\eta, \quad (A.14)$$

The lift distribution of Equation (A.6) can now be substituted in Equation (A.14). This gives:

$$\alpha(\xi_r, \eta_v) = \sum \sum -\frac{1}{2\pi A} \left[\frac{1}{2G_n} \int_{-1}^{+1} \frac{g_n(\eta)}{(\eta - \eta_v)^2} \left\{ \frac{1}{2H_q} \int_{-1}^{+1} h_q(\xi) K\{(x_r - x), (y_v - y)\} d\xi \right\} d\eta \right] \quad (A.15)$$

forming a set of linear simultaneous equations which can be written in matrix form as:

$$\{\alpha_v\} = [D_{rv}^n] \{P_n\} \quad \dots \quad (A.16)$$

The downwash vector, $\{\alpha_v\}$, is a column vector the elements of which are the streamwise slopes at the $(p \times m)$ downwash points, (ξ_r, η_v) . The square matrix $[D_{rv}^n]$ is the downwash influence coefficient matrix, element D_{rv}^n being the non-dimensional downwash at (ξ_r, η_v) induced by a unit equivalent load at (ξ_q, η_n) . To solve Equation (A.16) for the load vector we merely invert:

$$\{P_n\} = [D_{rv}^n]^{-1} \{\alpha_v\} , \quad \dots \quad (A.17)$$

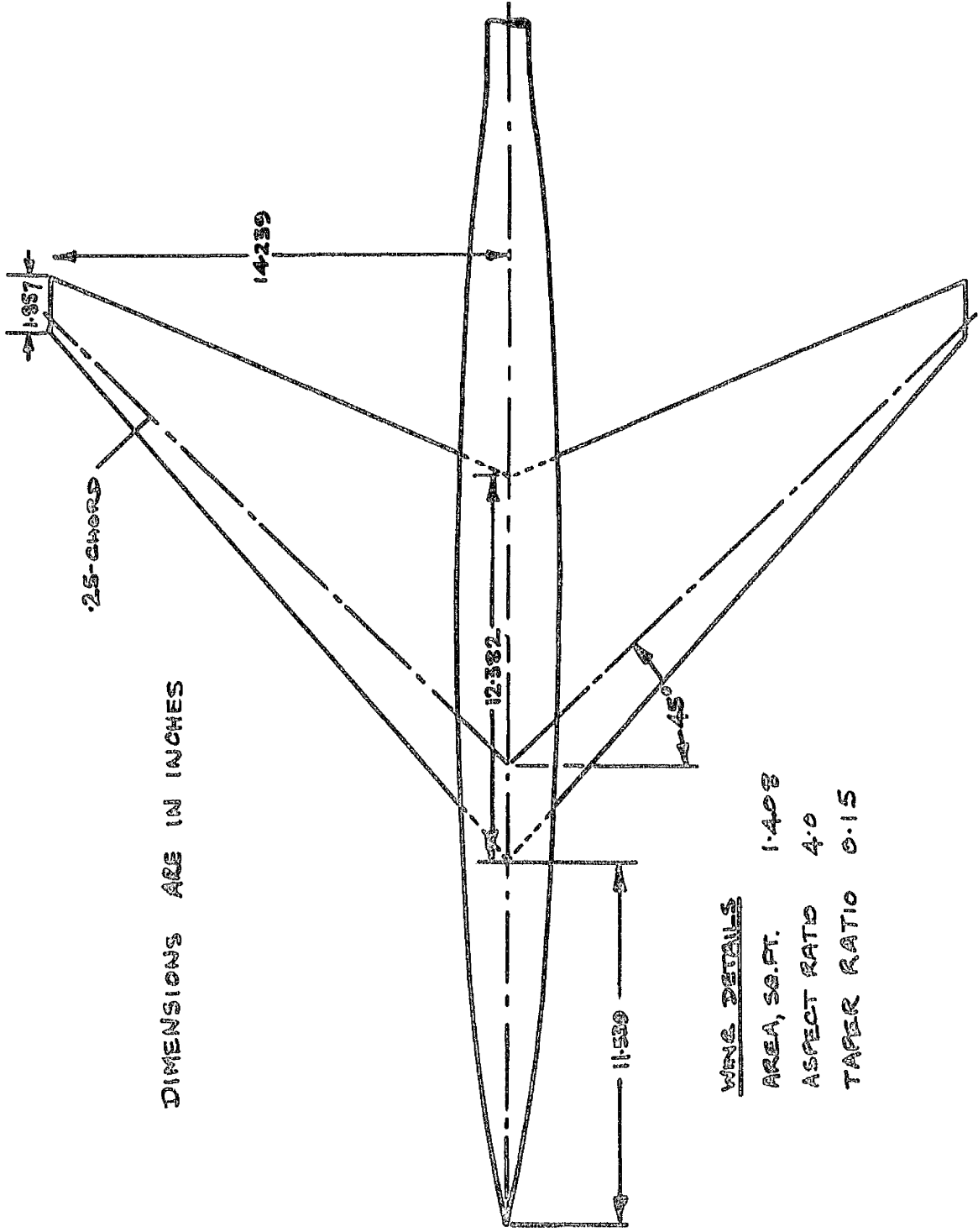
$$= [A_{qv}^r] \{\alpha_v\} , \quad \dots \quad (A.18)$$

or more conveniently,

$$\{P\} = [A] \{\alpha\} \quad \dots \quad (A.19)$$

Element A_{rs} is now the equivalent load at (ξ_s, η_s) induced by a unit downwash at (ξ_r, η_r) .

Standard Deuce programmes exist which calculate the elements of matrix $[A]$ for the symmetric and antisymmetric downwash conditions.



DIMENSIONS ARE IN INCHES

FIGURE 1 :- DETAILS OF MODEL WITH DIFFERENT BUILT-IN SPANWISE TWIST DISTRIBUTIONS .

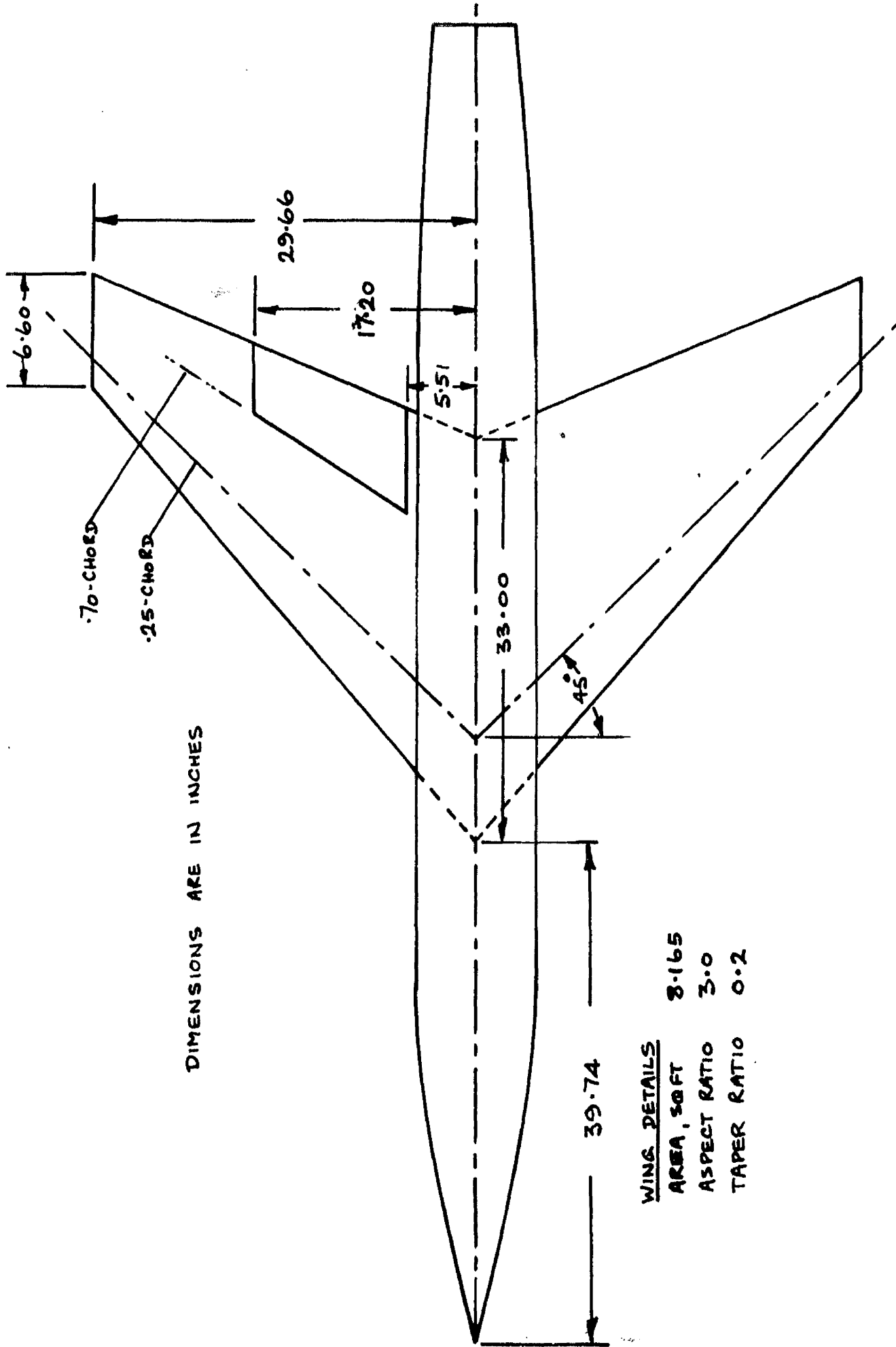


FIGURE 2:-- DETAILS OF MODEL WITHAILERON ON STARBOARD SEMISPAN

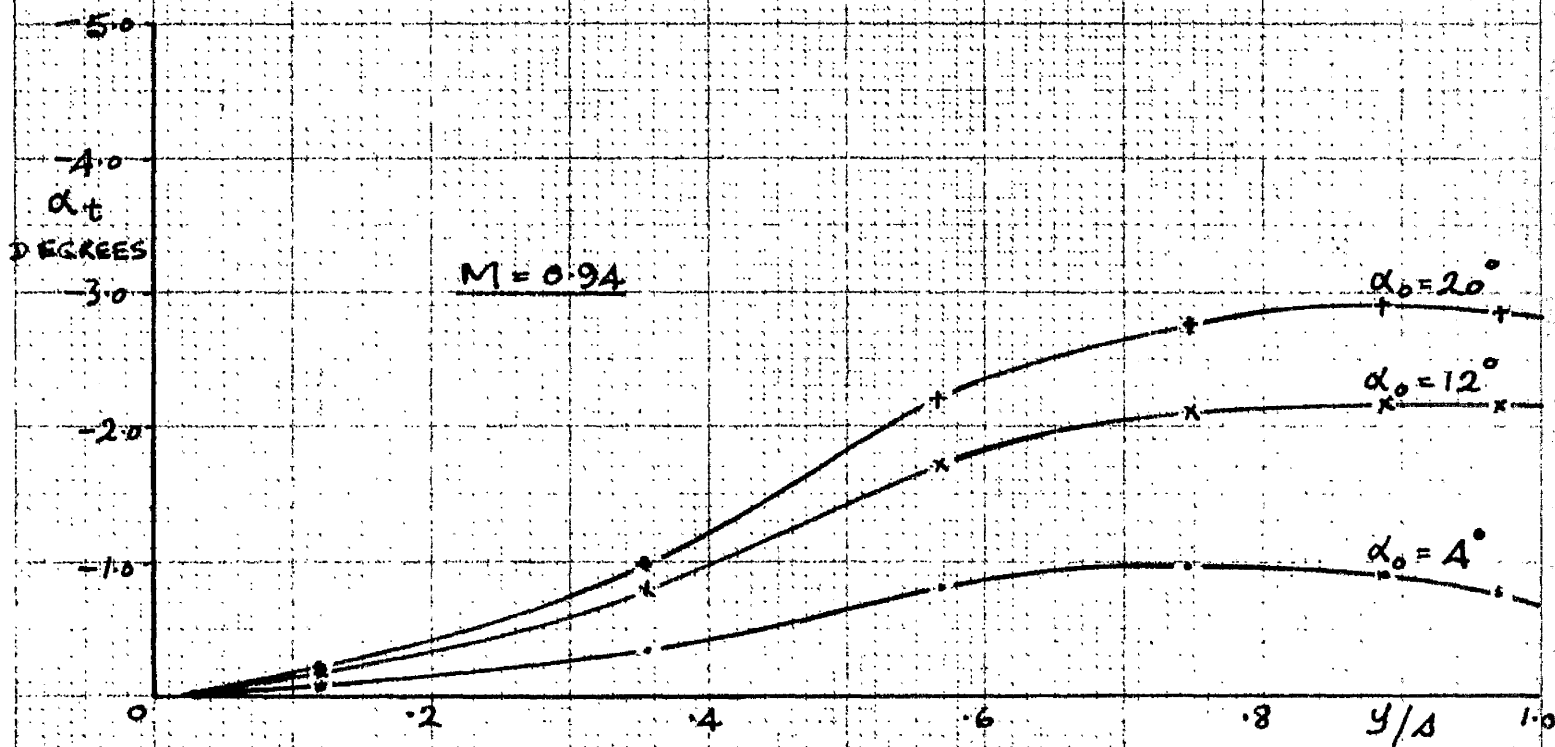
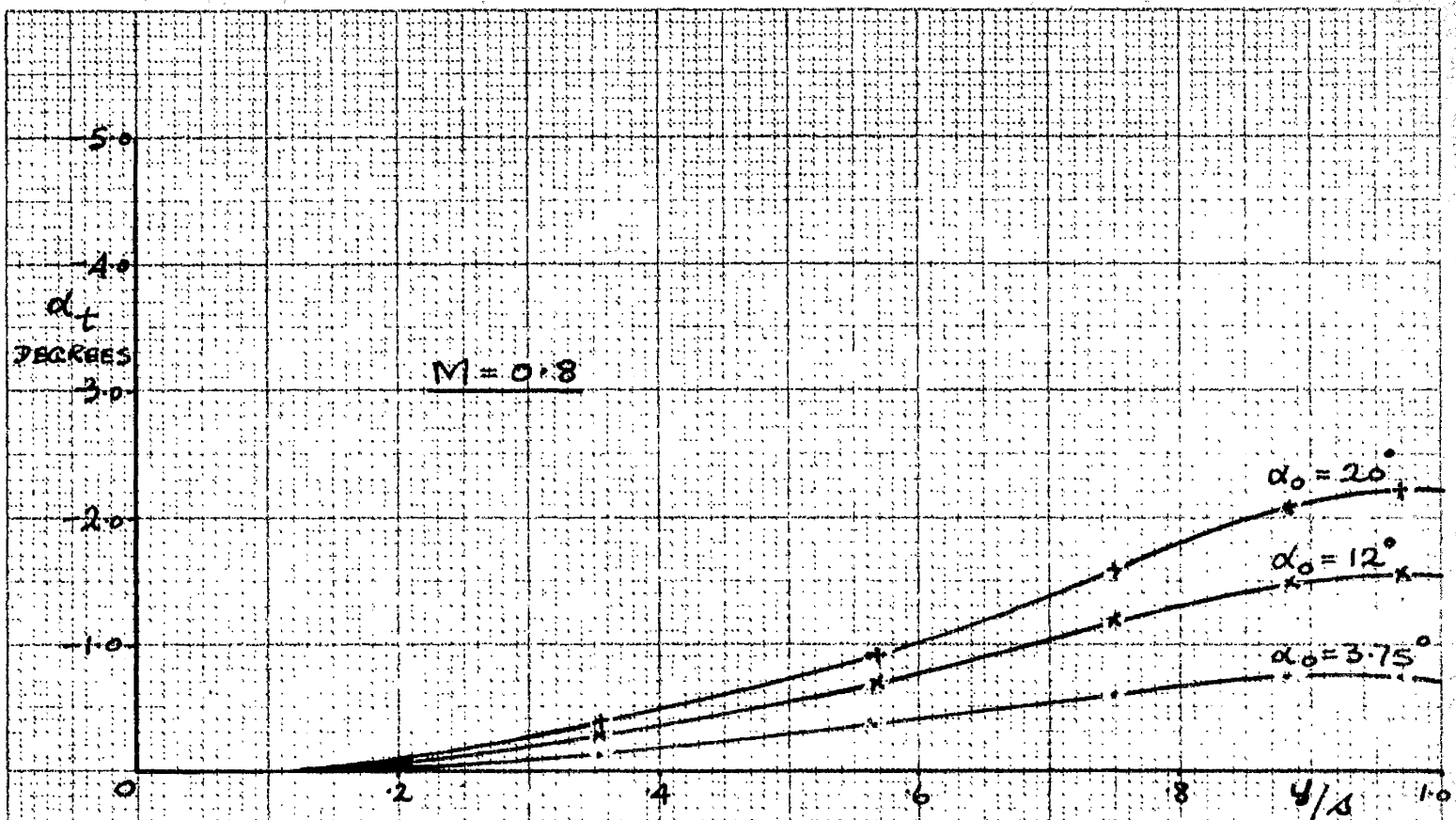


FIGURE 3a :- SPANWISE TWIST DISTRIBUTIONS FOR THE PLANAR WING I.

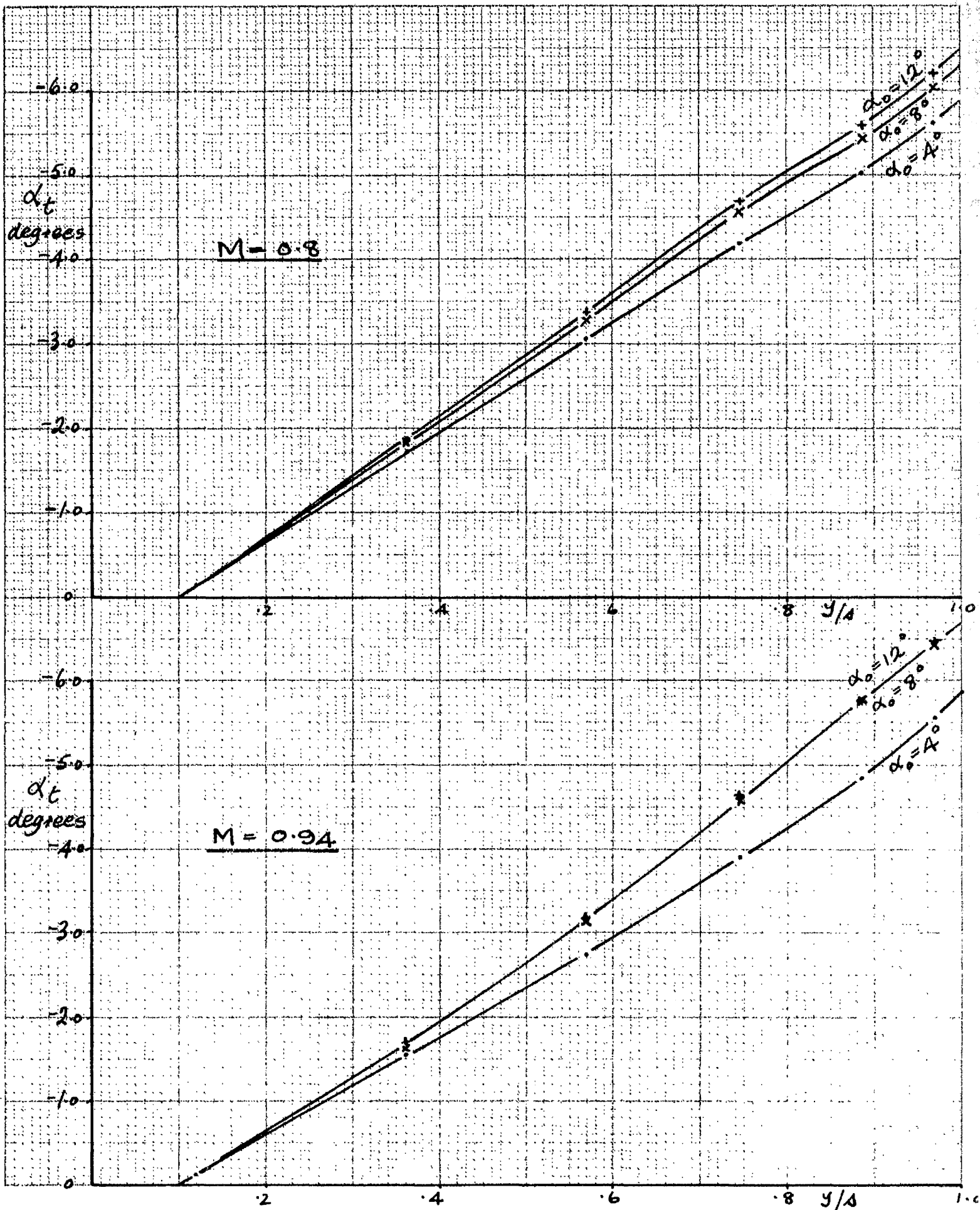


FIGURE 3b :- SPANWISE TWIST DISTRIBUTIONS FOR THE LINEAR WING .

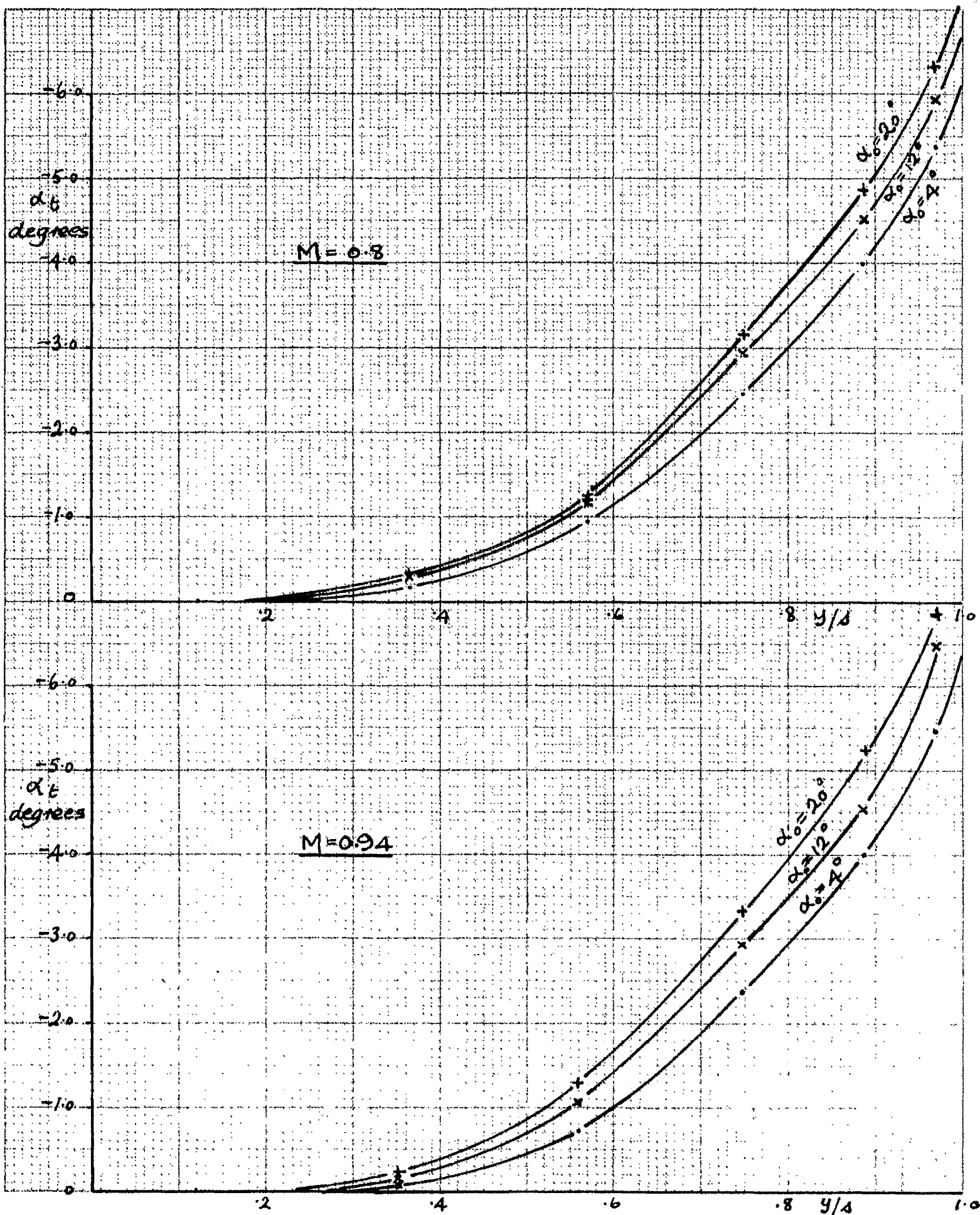


FIGURE 3c :- SPANWISE TWIST DISTRIBUTIONS FOR THE CUBIC WING.

————— THEORY

----- EXPERIMENT (REF. 12)

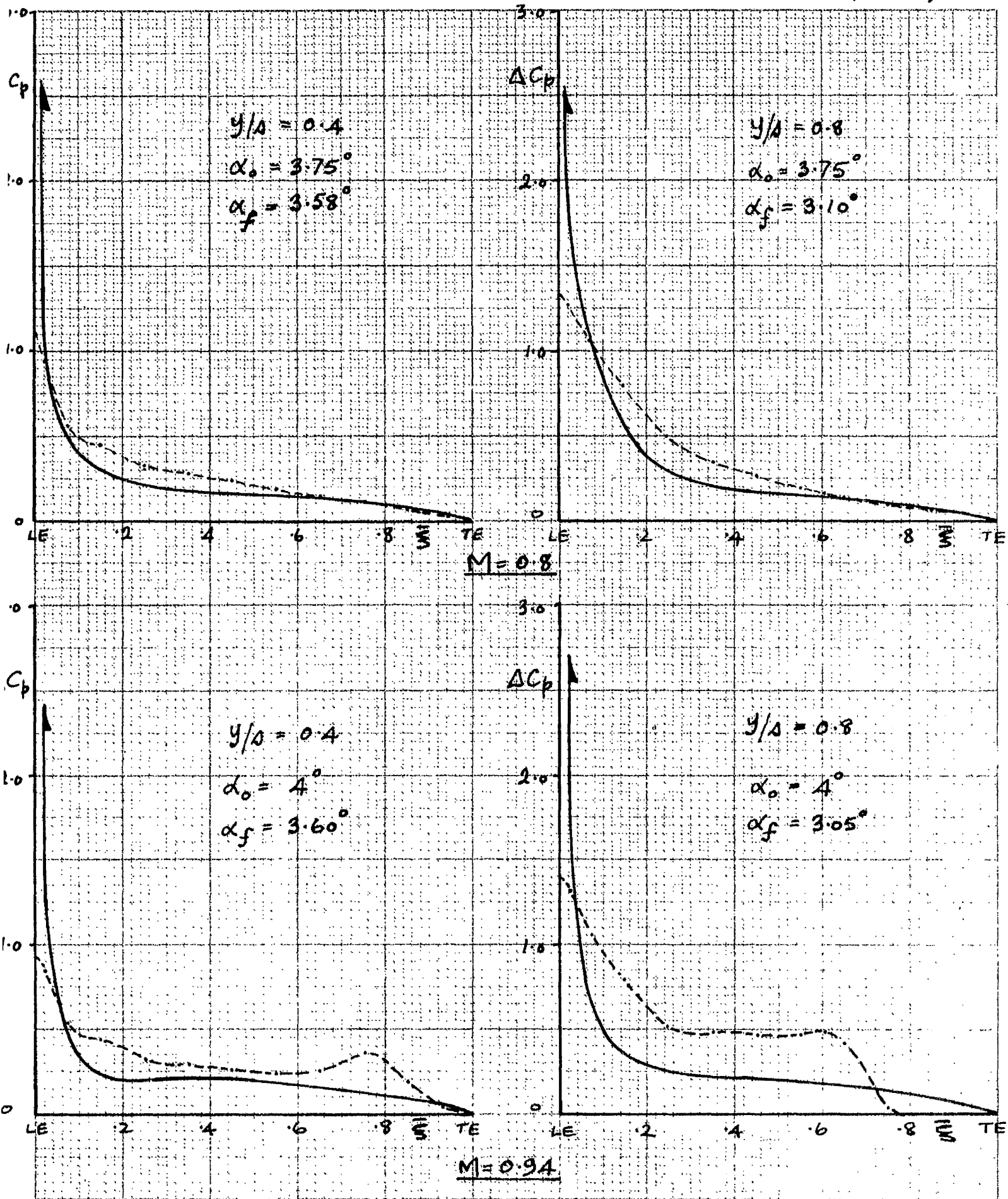


FIGURE 4a: — COMPARISON OF THE THEORETICAL AND EXPERIMENTAL CHORDWISE PRESSURE DISTRIBUTIONS FOR THE PLANAR WING I AT $M = 0.8$ AND $M = 0.94$.

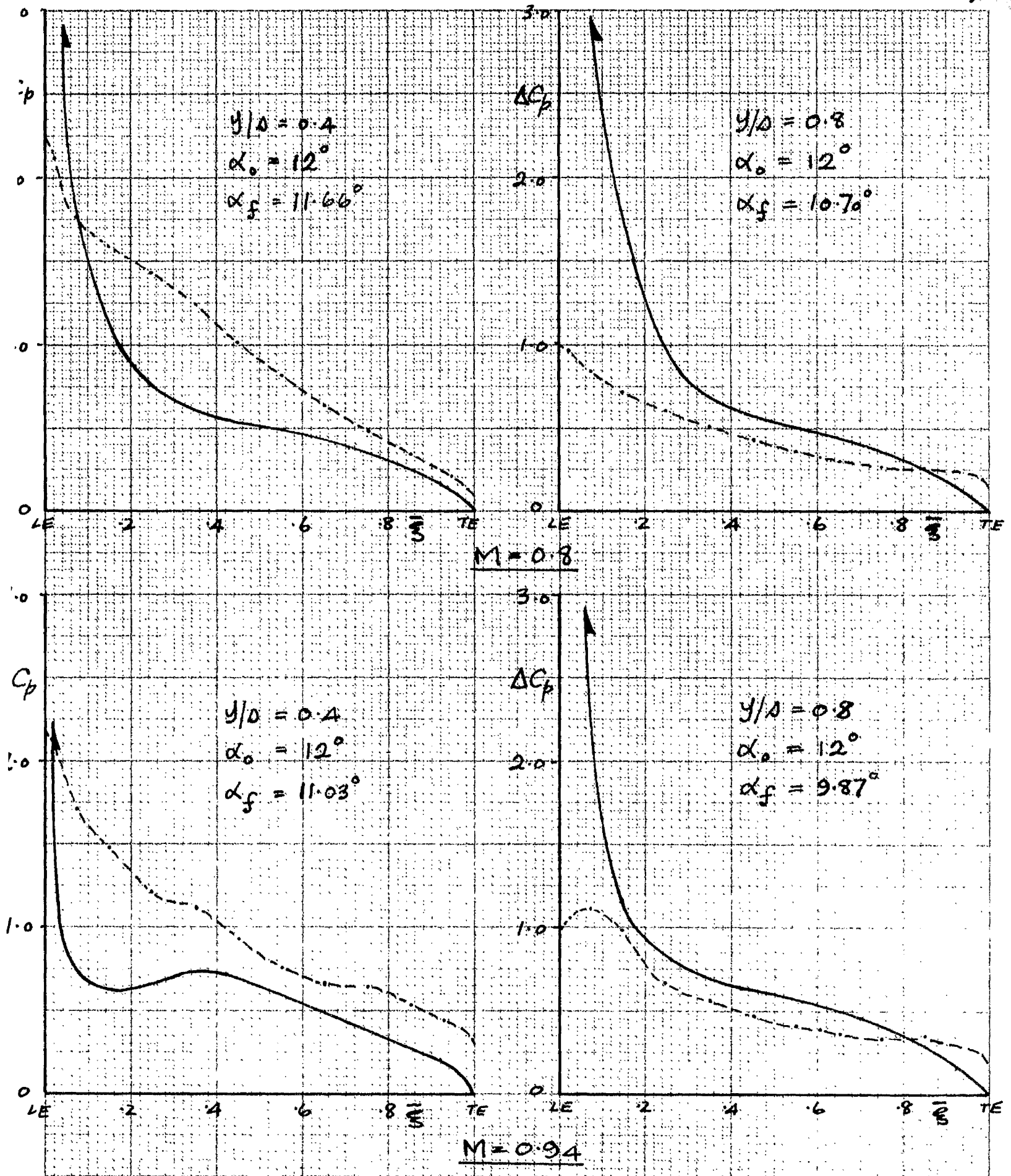


FIGURE 4b :- COMPARISON OF THE THEORETICAL AND EXPERIMENTAL CHORDWISE PRESSURE DISTRIBUTIONS FOR THE PLANAR WING I AT $M = 0.8$ AND $M = 0.94$.

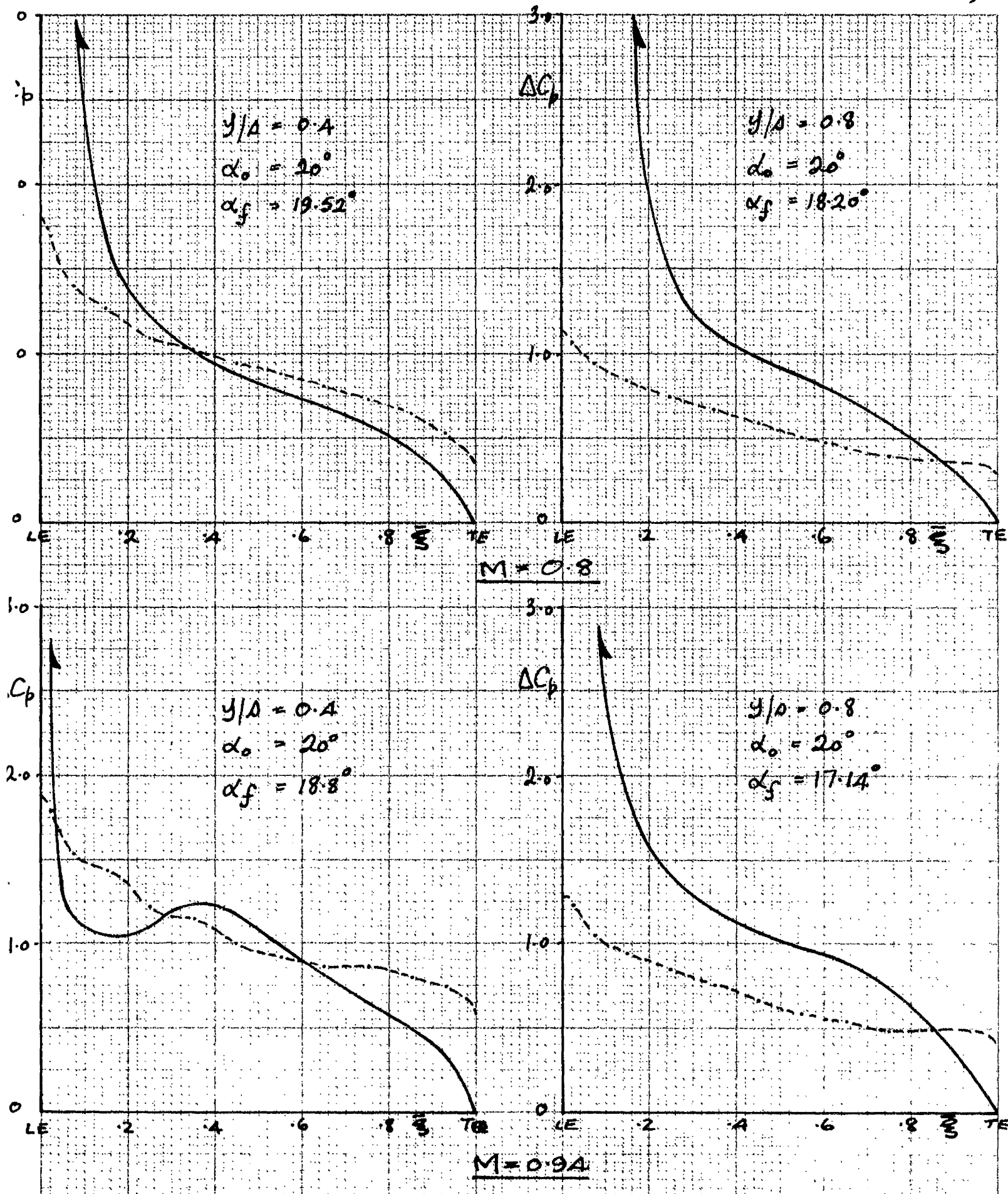


FIGURE 4C: - COMPARISON OF THE THEORETICAL AND EXPERIMENTAL CHORDWISE PRESSURE DISTRIBUTIONS FOR THE PLANAR WING I AT $M = 0.8$ AND $M = 0.94$.

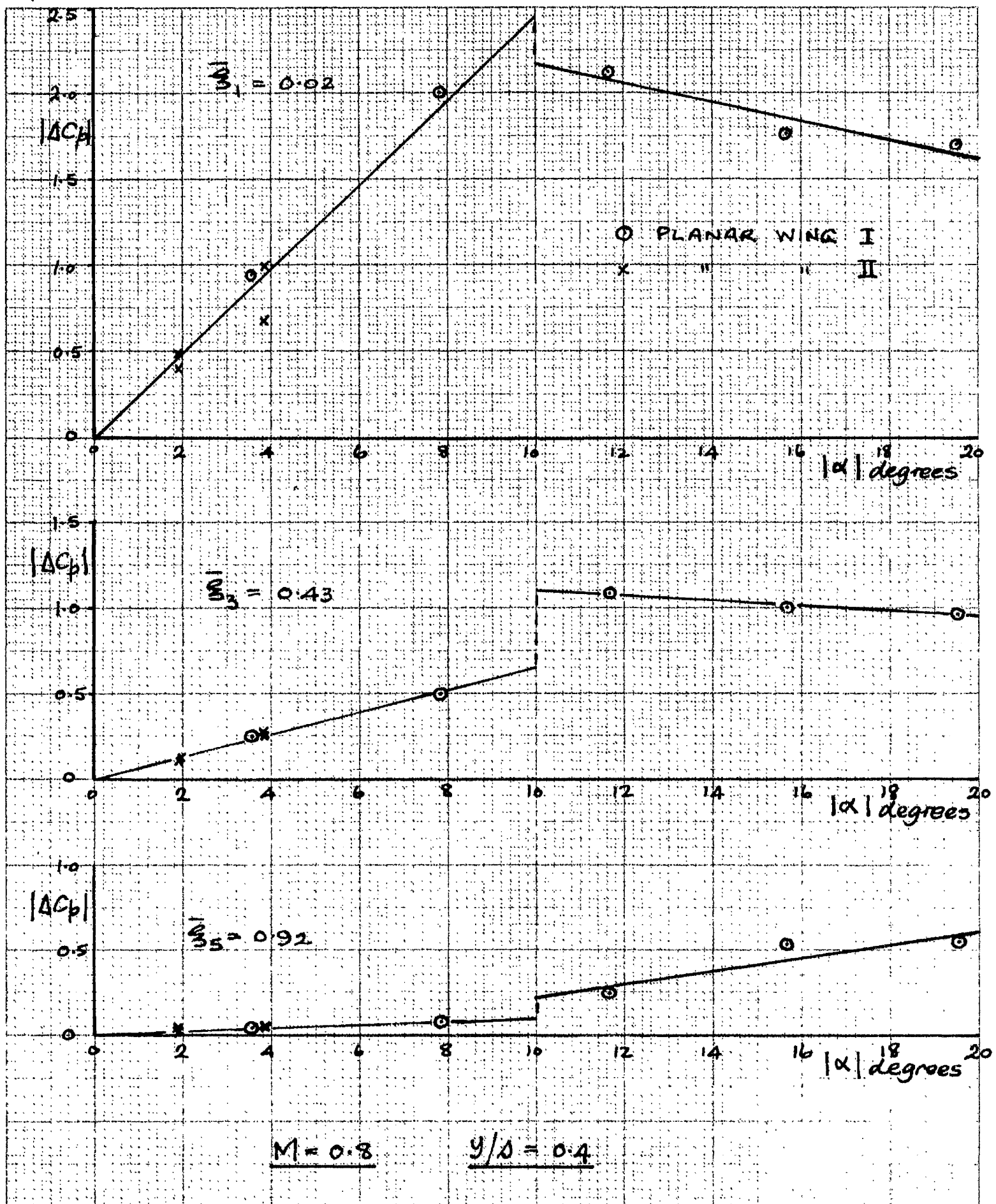


FIGURE 5a:- PLANAR WING PRESSURE COEFFICIENT AGAINST LOCAL WING SLOPE (POINT THEORY).

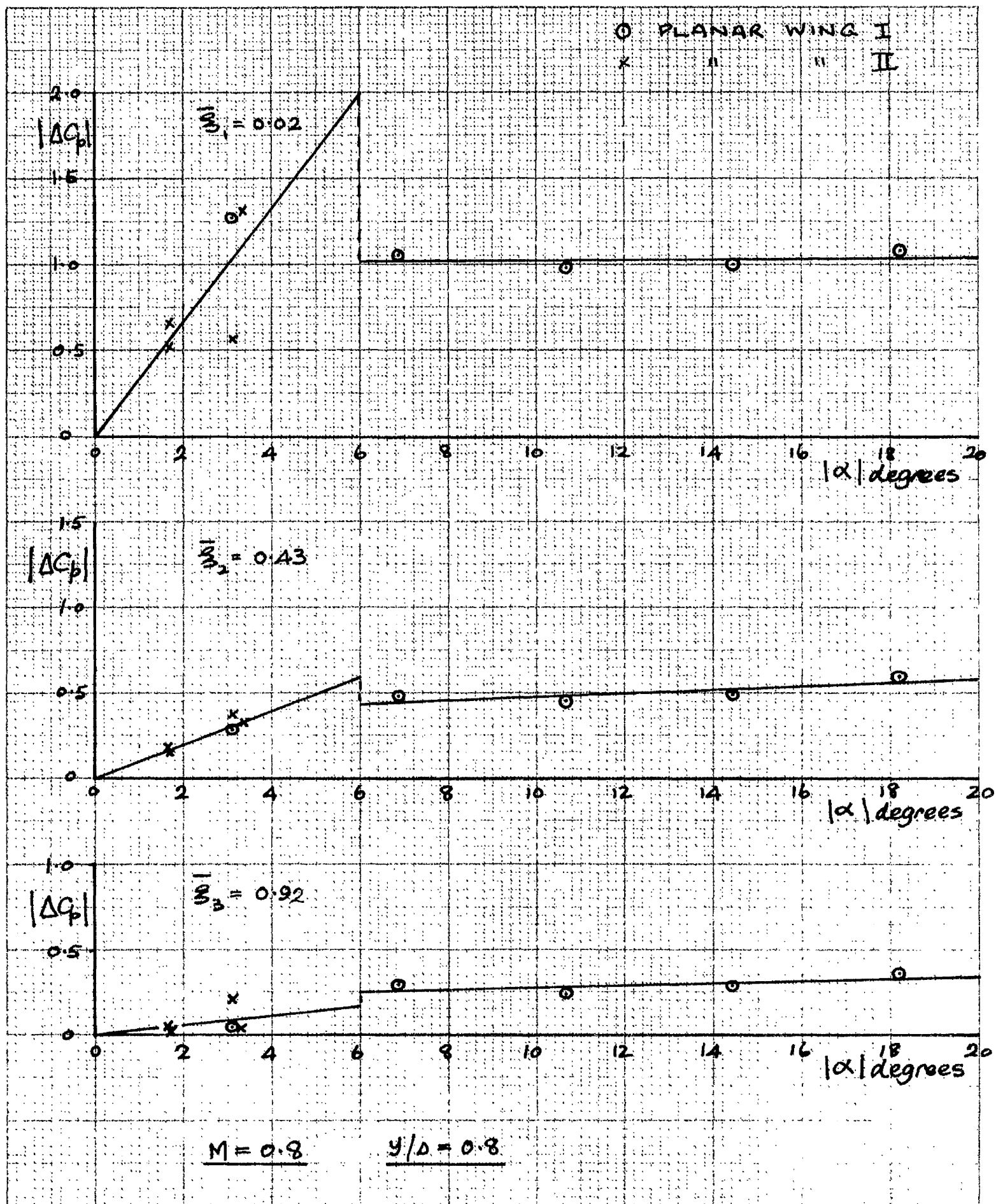


FIGURE 5b :- PLANAR WING PRESSURE COEFFICIENT AGAINST LOCAL WING SLOPE (POINT THEORY).

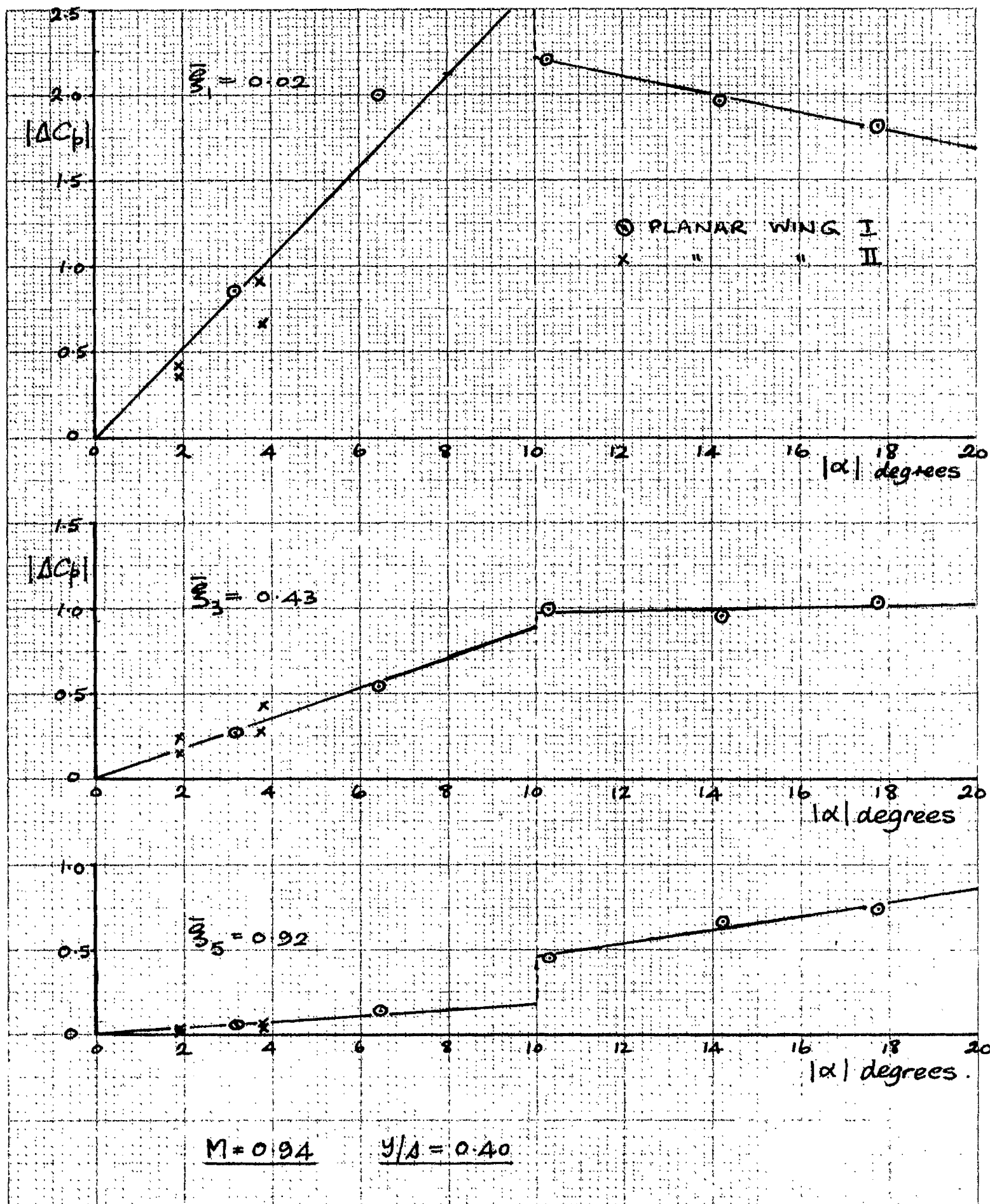


FIGURE 5C :- PLANAR WING PRESSURE COEFFICIENT AGAINST LOCAL WING SLOPE (POINT THEORY).

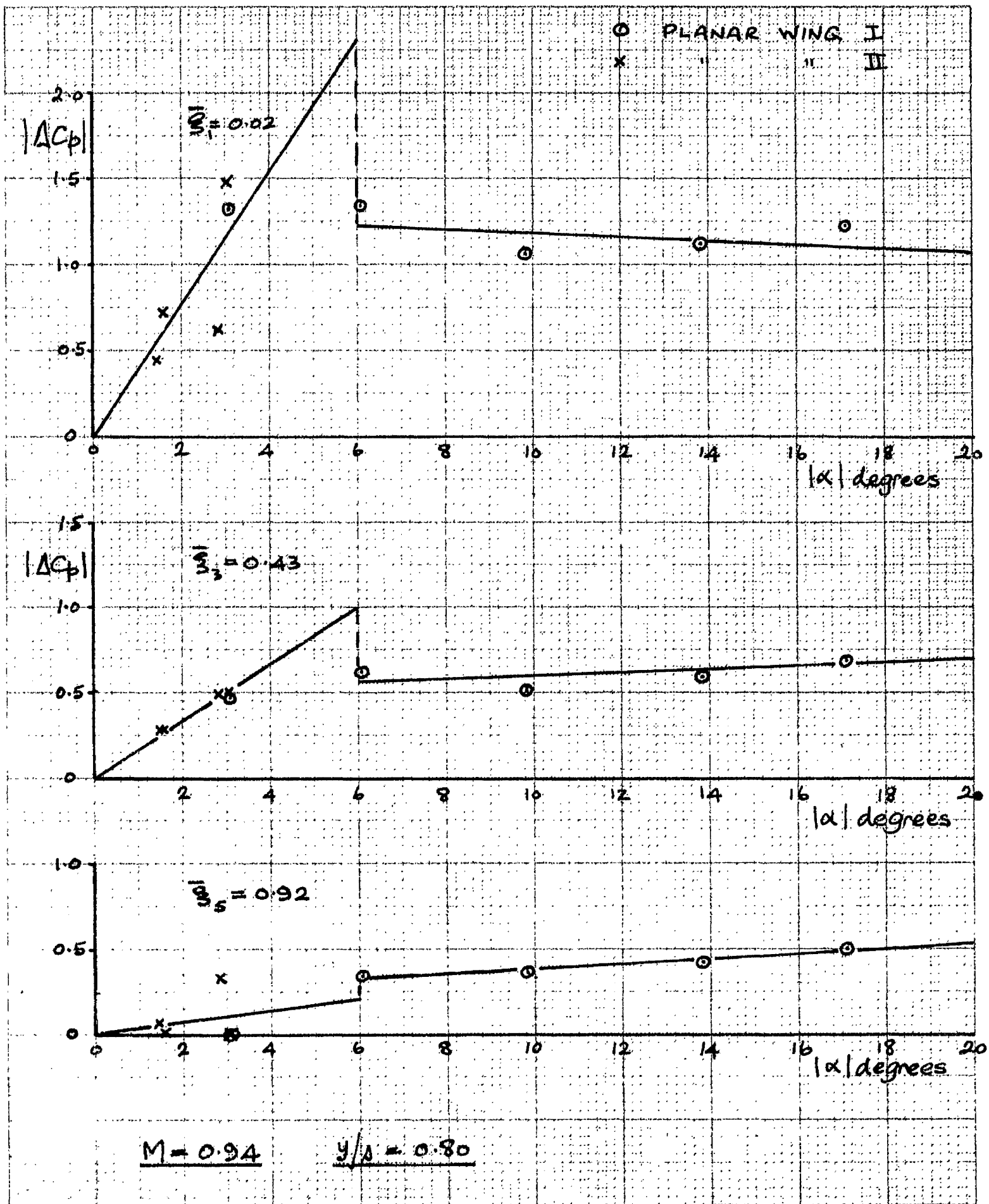


FIGURE 5d :- PLANAR WING PRESSURE COEFFICIENT AGAINST LOCAL WING SLOPE (POINT THEORY).

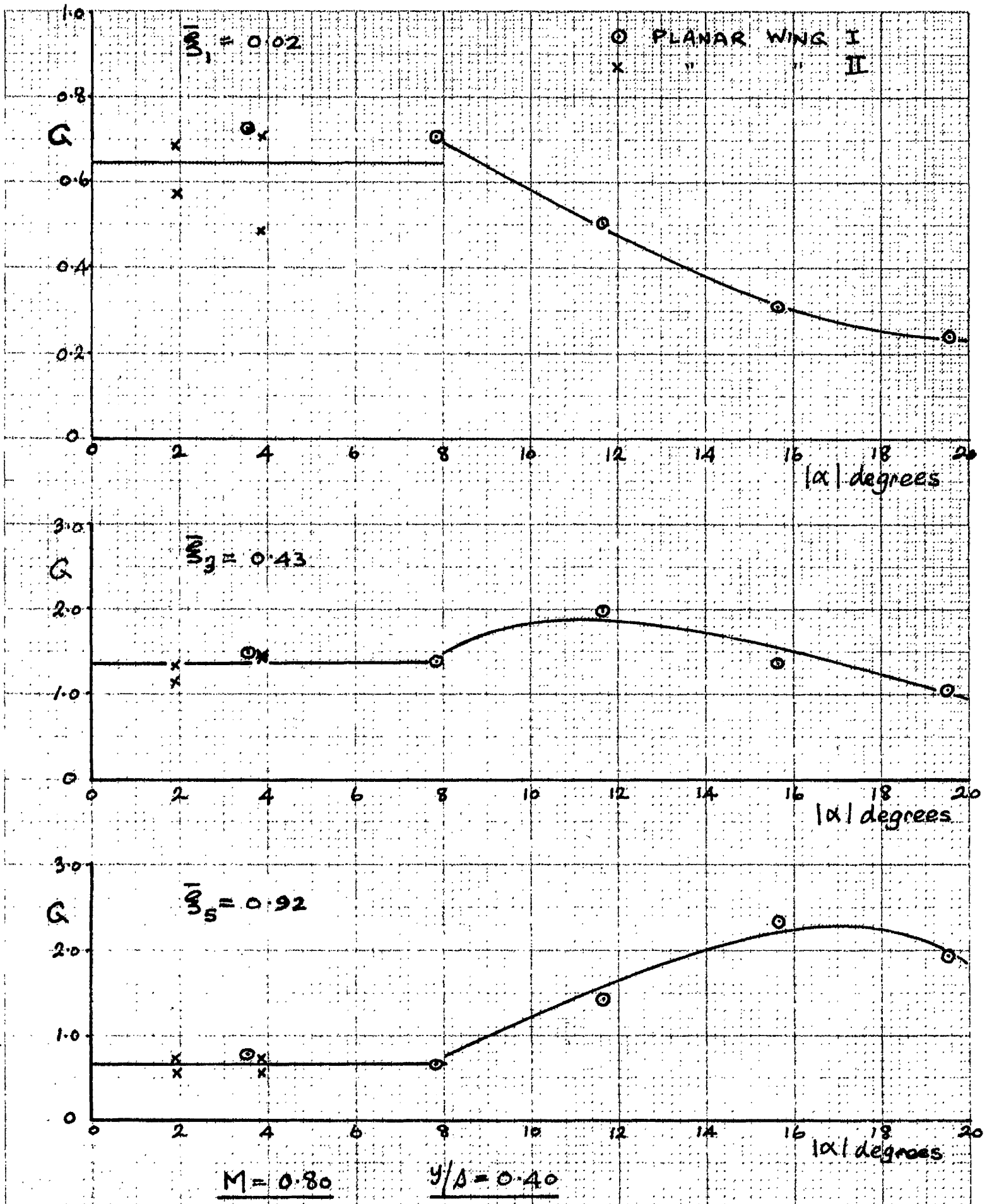


FIGURE 6a :- CORRECTION FACTORS FOR METHOD II.

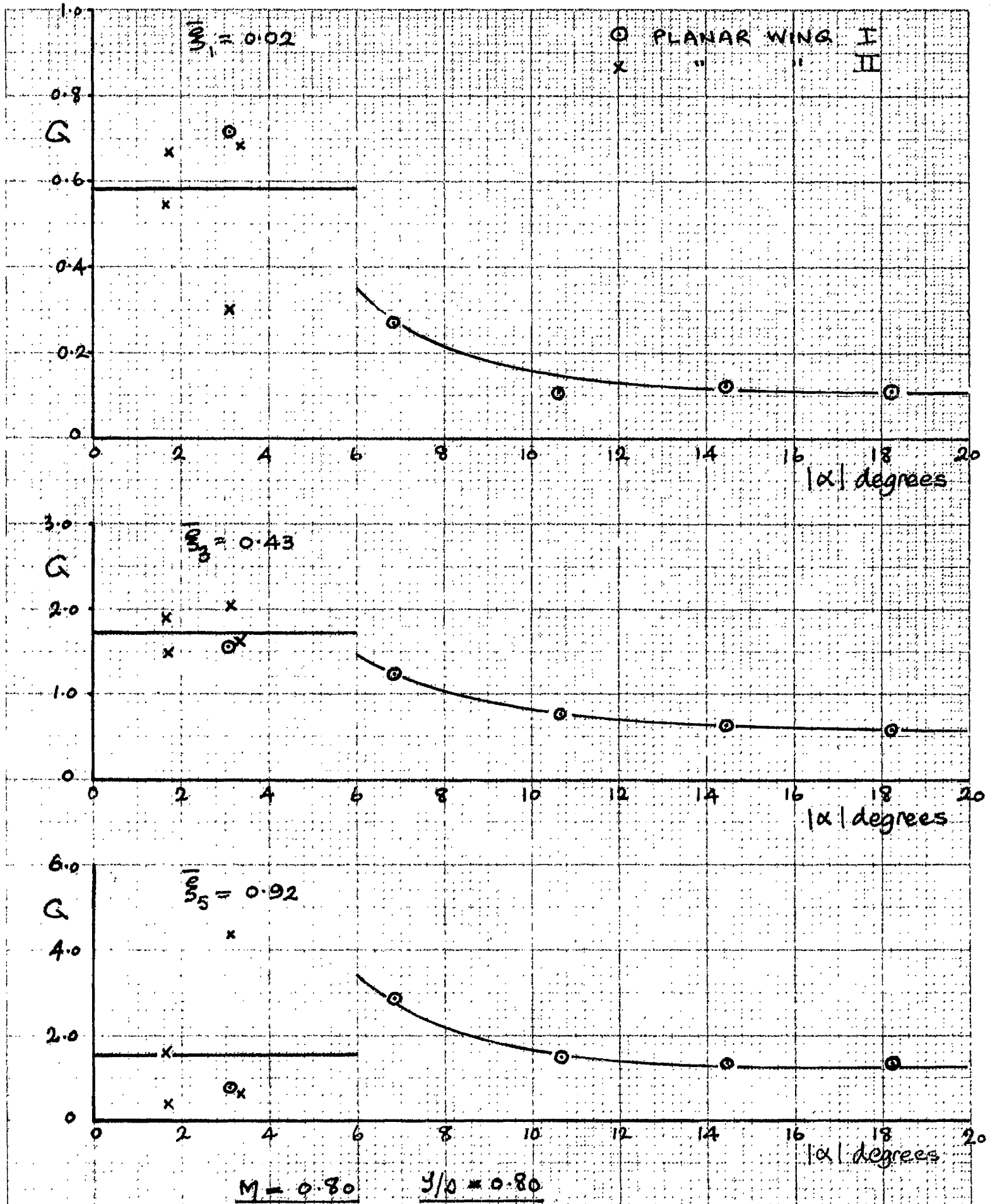


FIGURE 6b :- CORRECTION FACTORS FOR METHOD II.

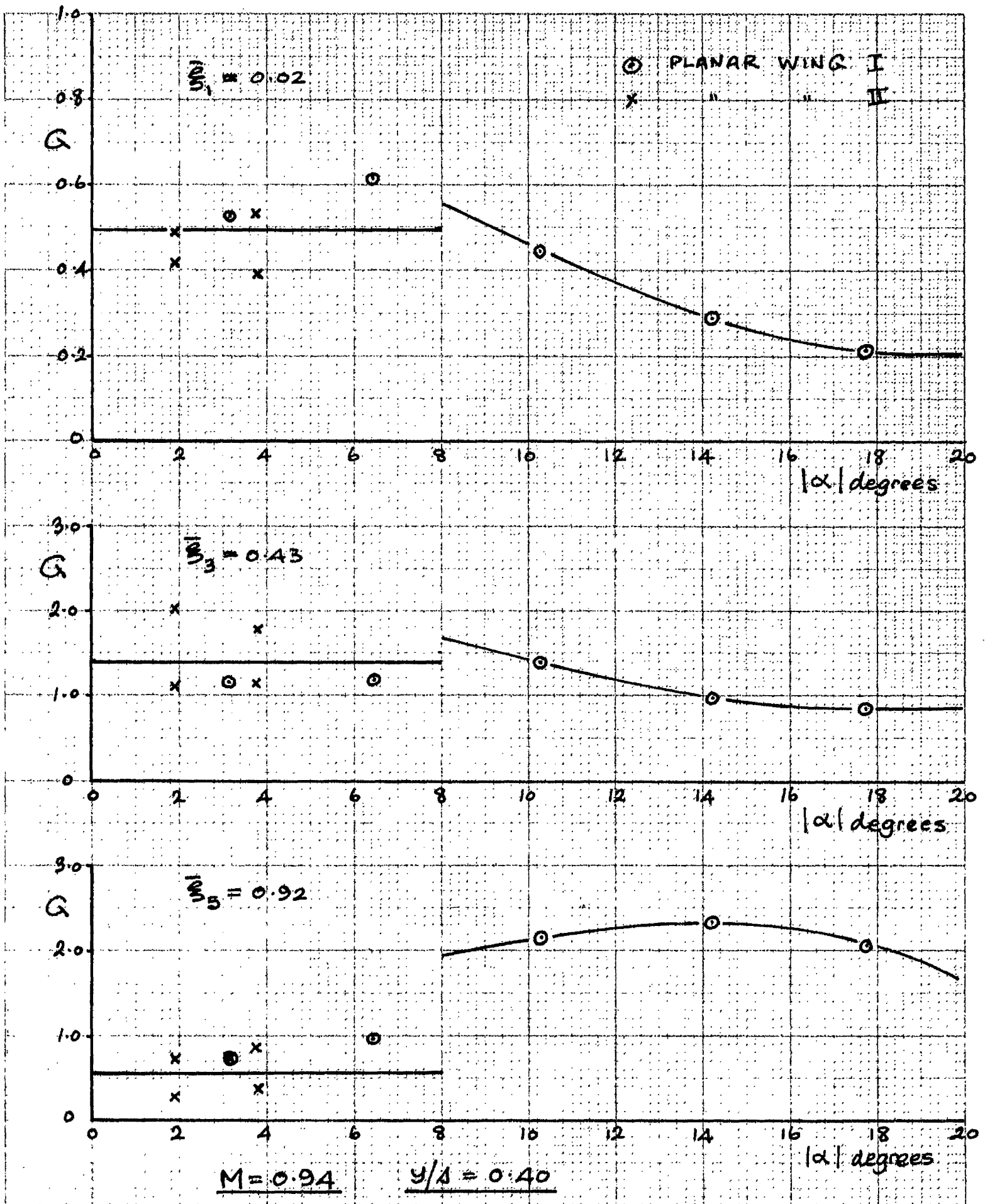


FIGURE 6C :- CORRECTION FACTORS FOR METHOD II.

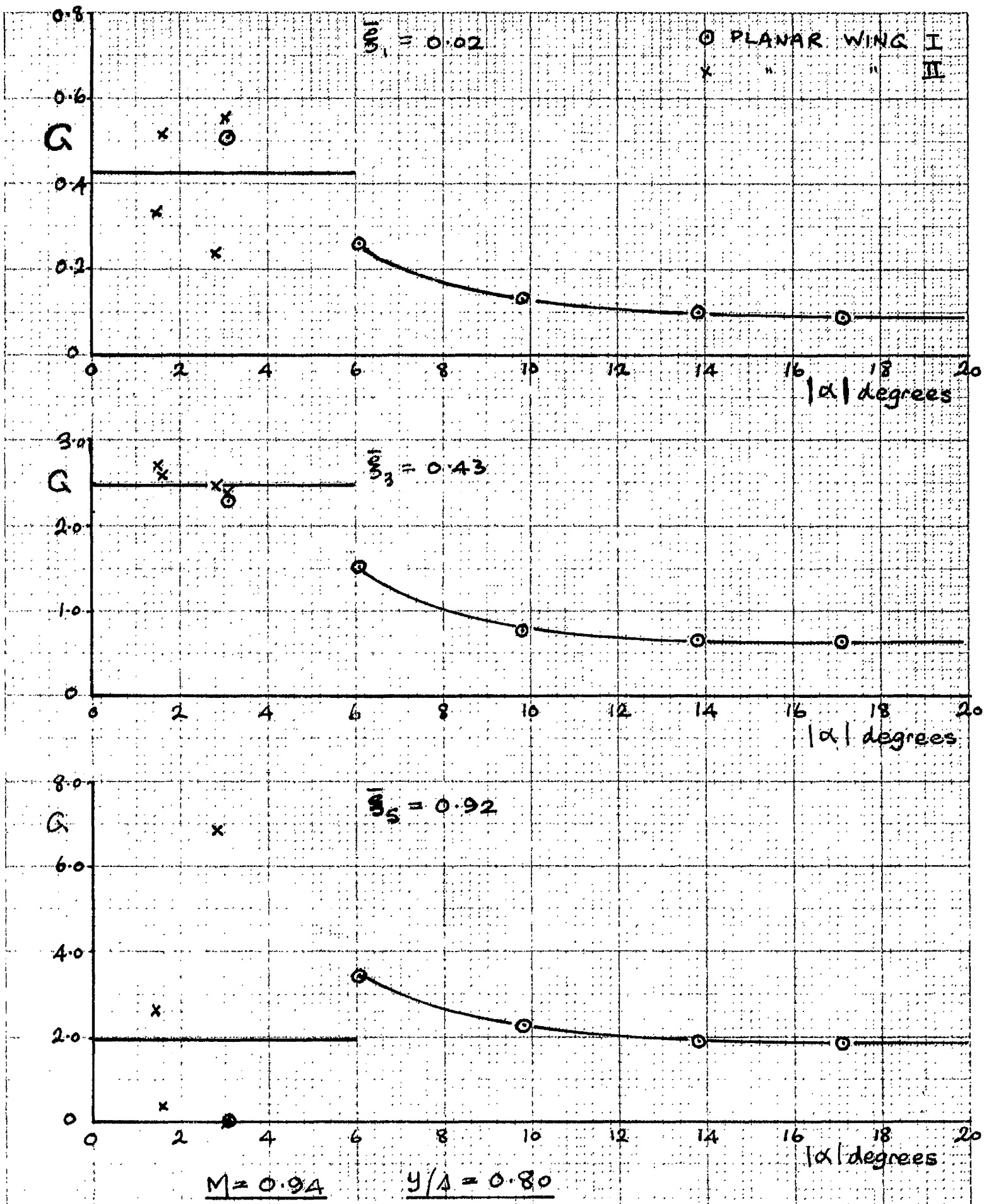


FIGURE 6d :- CORRECTION FACTORS FOR METHOD II.

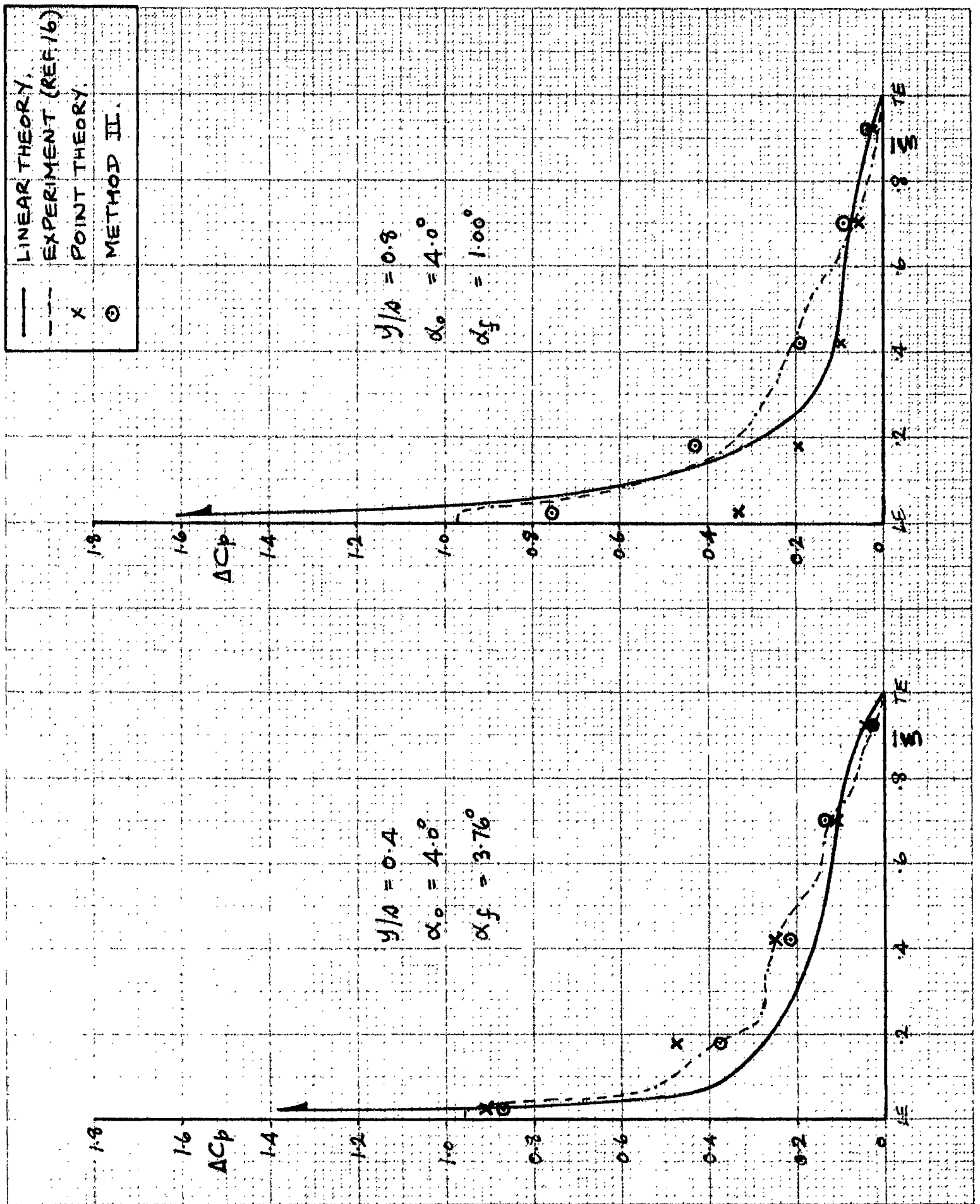


FIGURE 7a :- CUBIC WING MODIFIED PRESSURE DISTRIBUTION.
 $M = 0.8.$

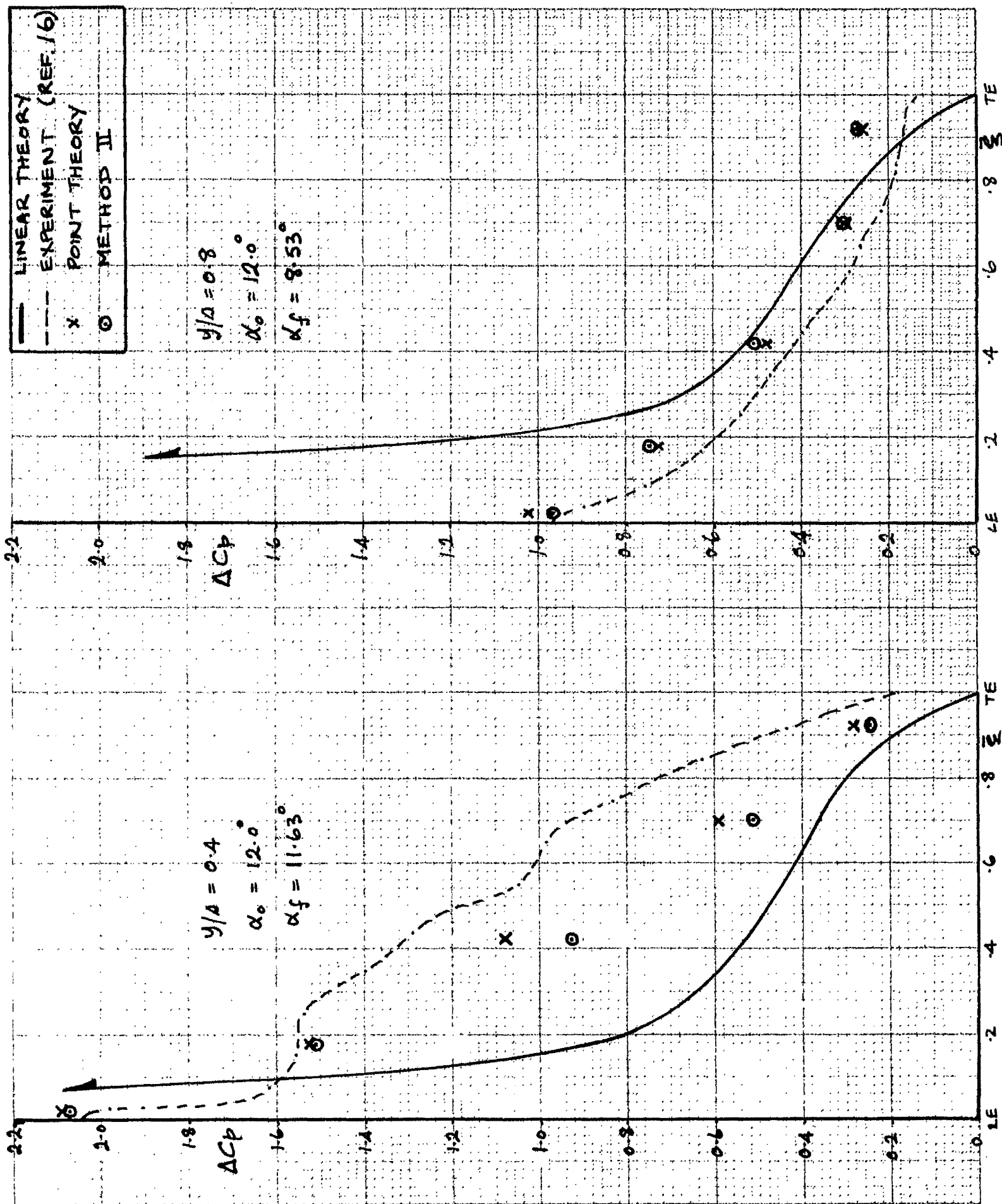


FIGURE 7b :- CUBIC WING MODIFIED PRESSURE DISTRIBUTION.
 M = 0.8.

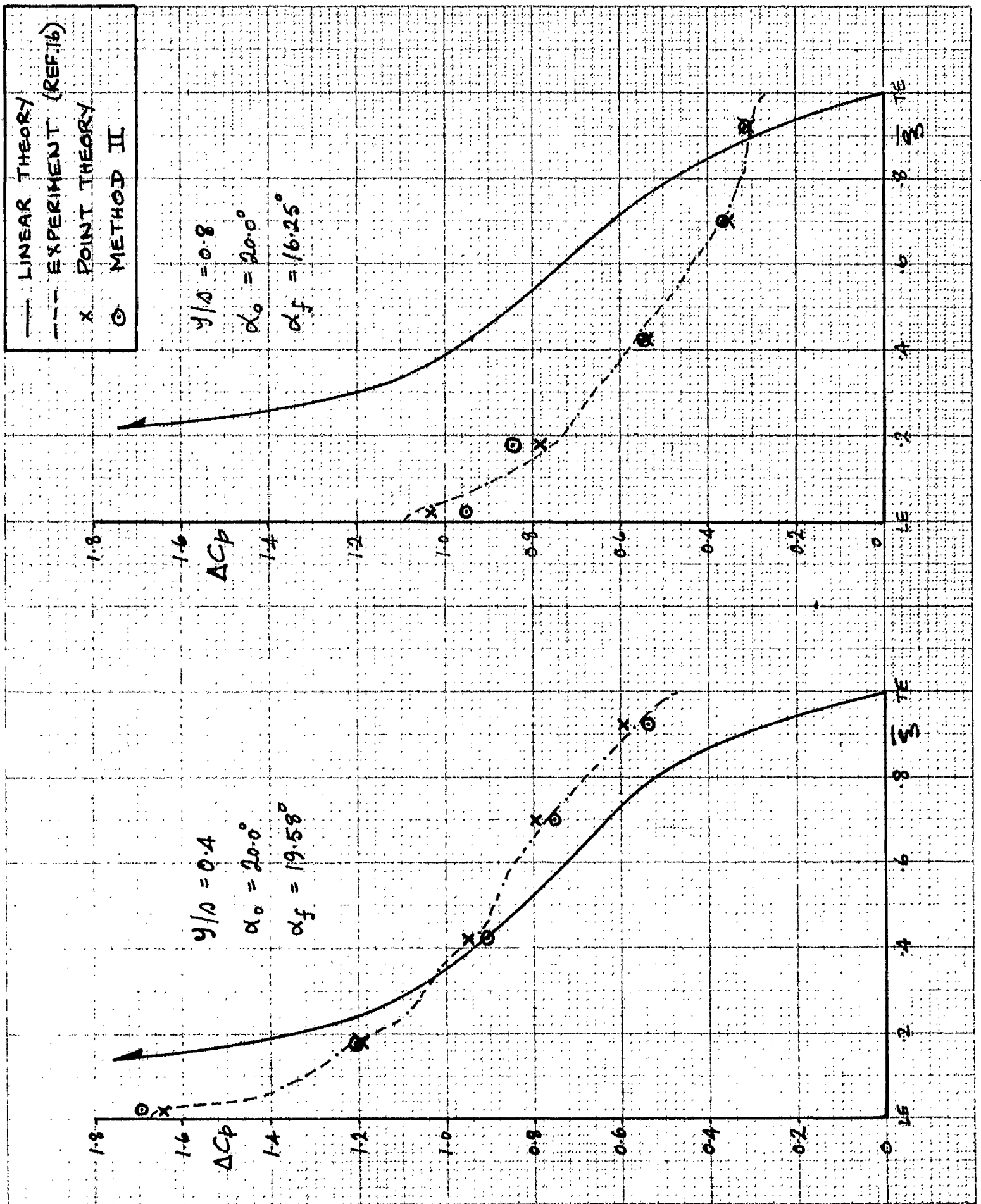


FIGURE 7C :- CUBIC WING MODIFIED PRESSURE DISTRIBUTION.
 $M = 0.8.$

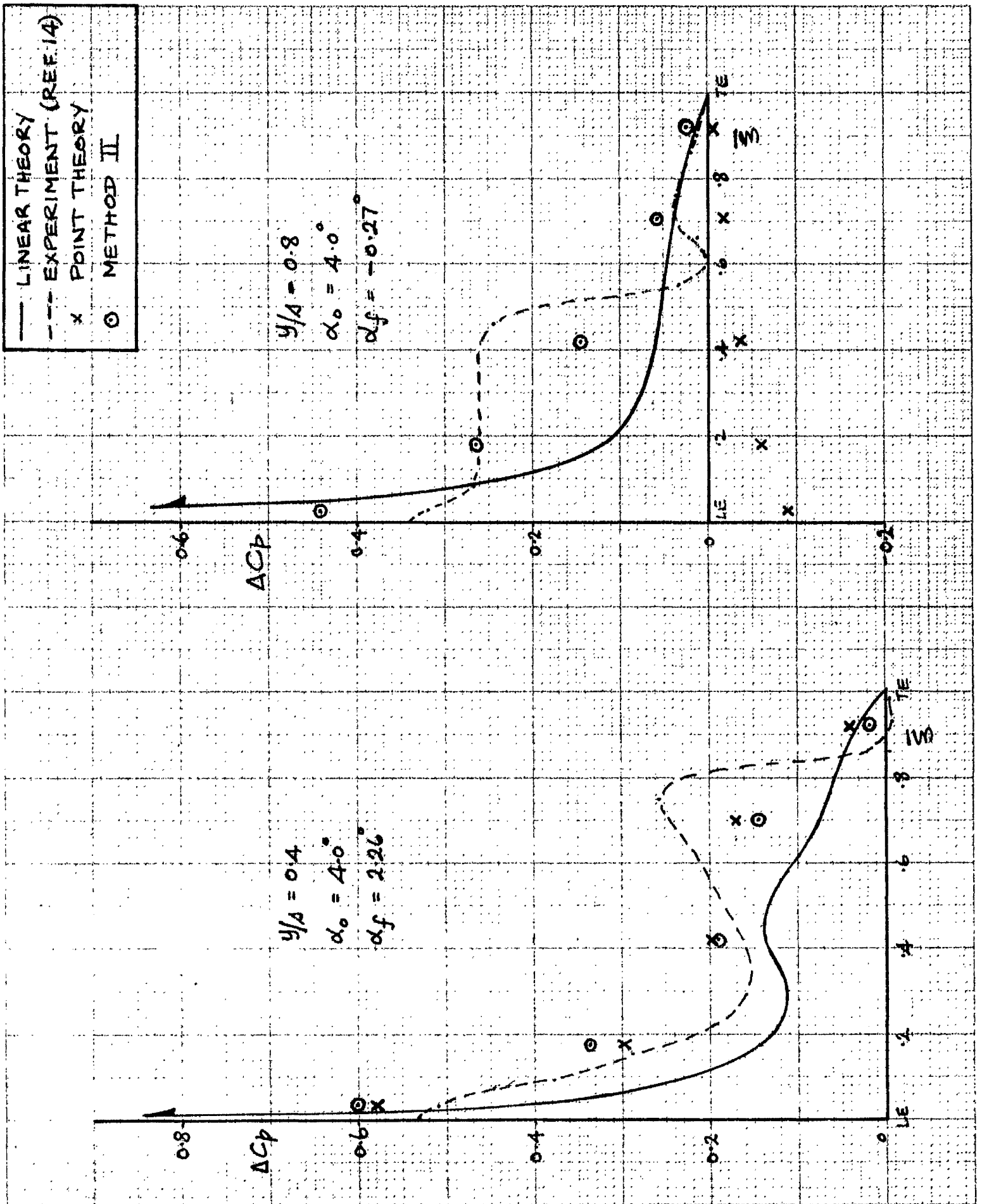


FIGURE 8a :- LINEAR WING MODIFIED PRESSURE DISTRIBUTION.
 $M = 0.94$.

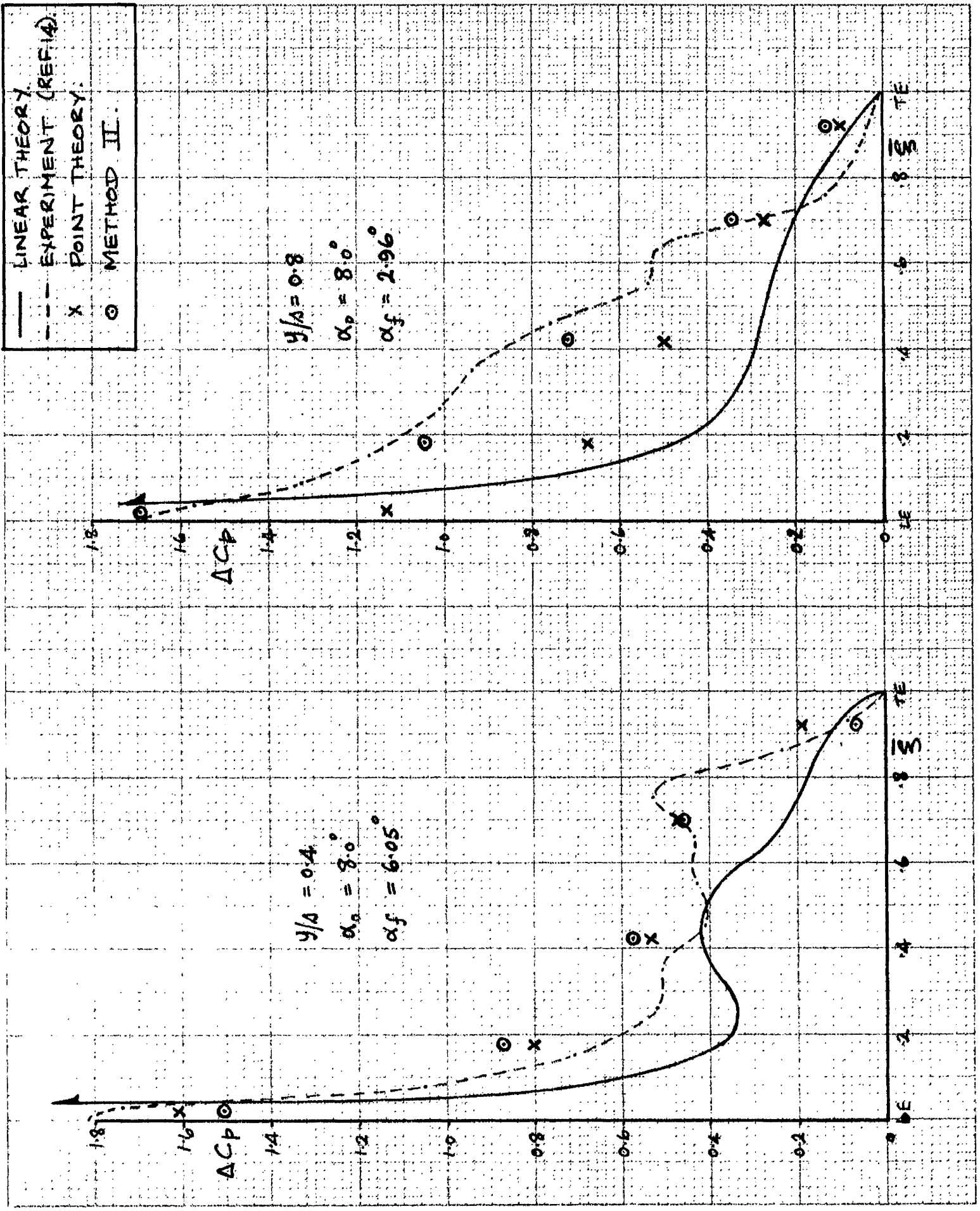


FIGURE 8b :- LINEAR WING MODIFIED PRESSURE DISTRIBUTION.
 $M = 0.94.$

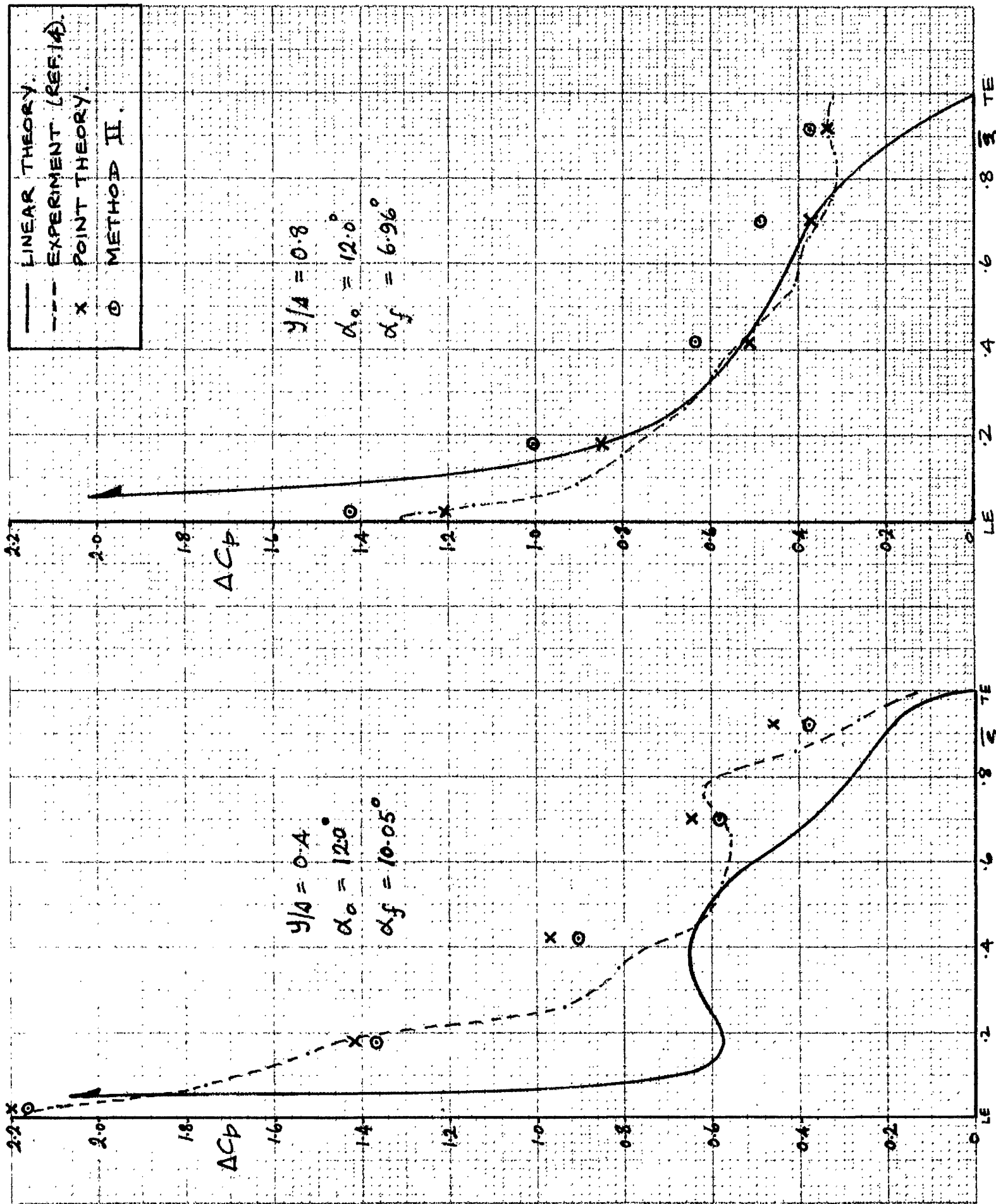


FIGURE 8C:— LINEAR WING MODIFIED PRESSURE DISTRIBUTION.
 $M = 0.94$.

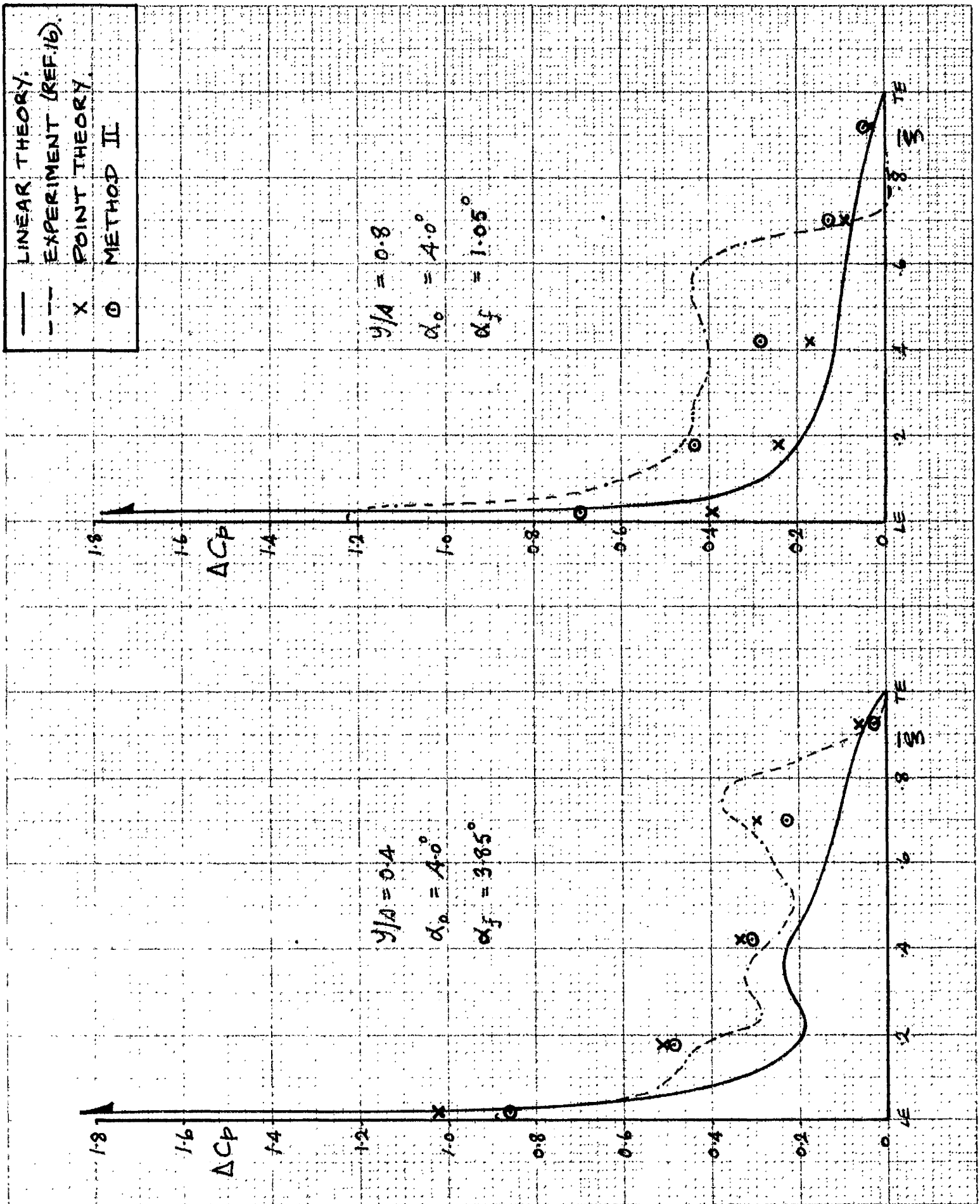


FIGURE 9a :- CUBIC WING MODIFIED PRESSURE DISTRIBUTION.
 $M = 0.94$.

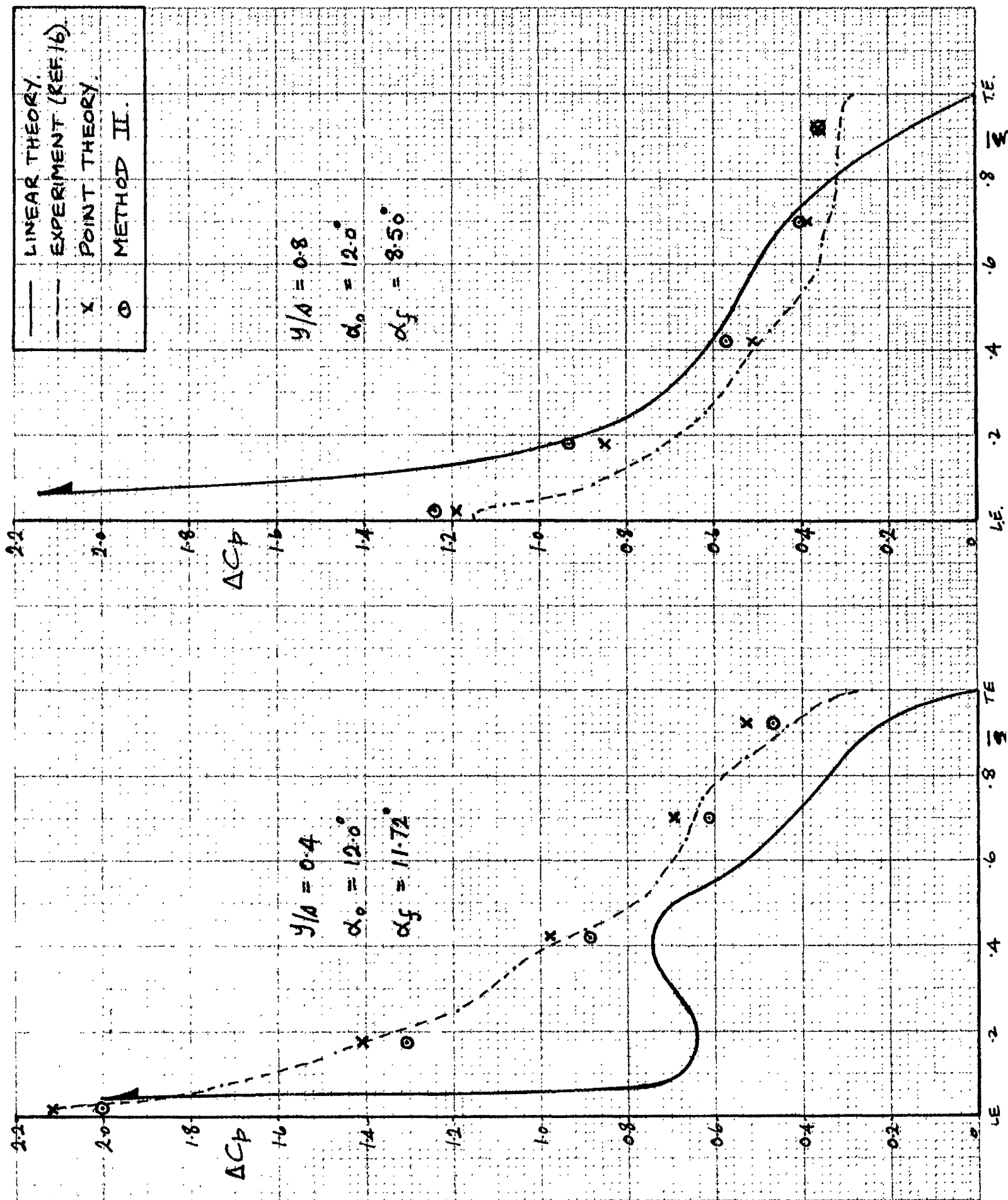


FIGURE 9b:- CUBIC WING MODIFIED PRESSURE DISTRIBUTION.
 $M = 0.94$.

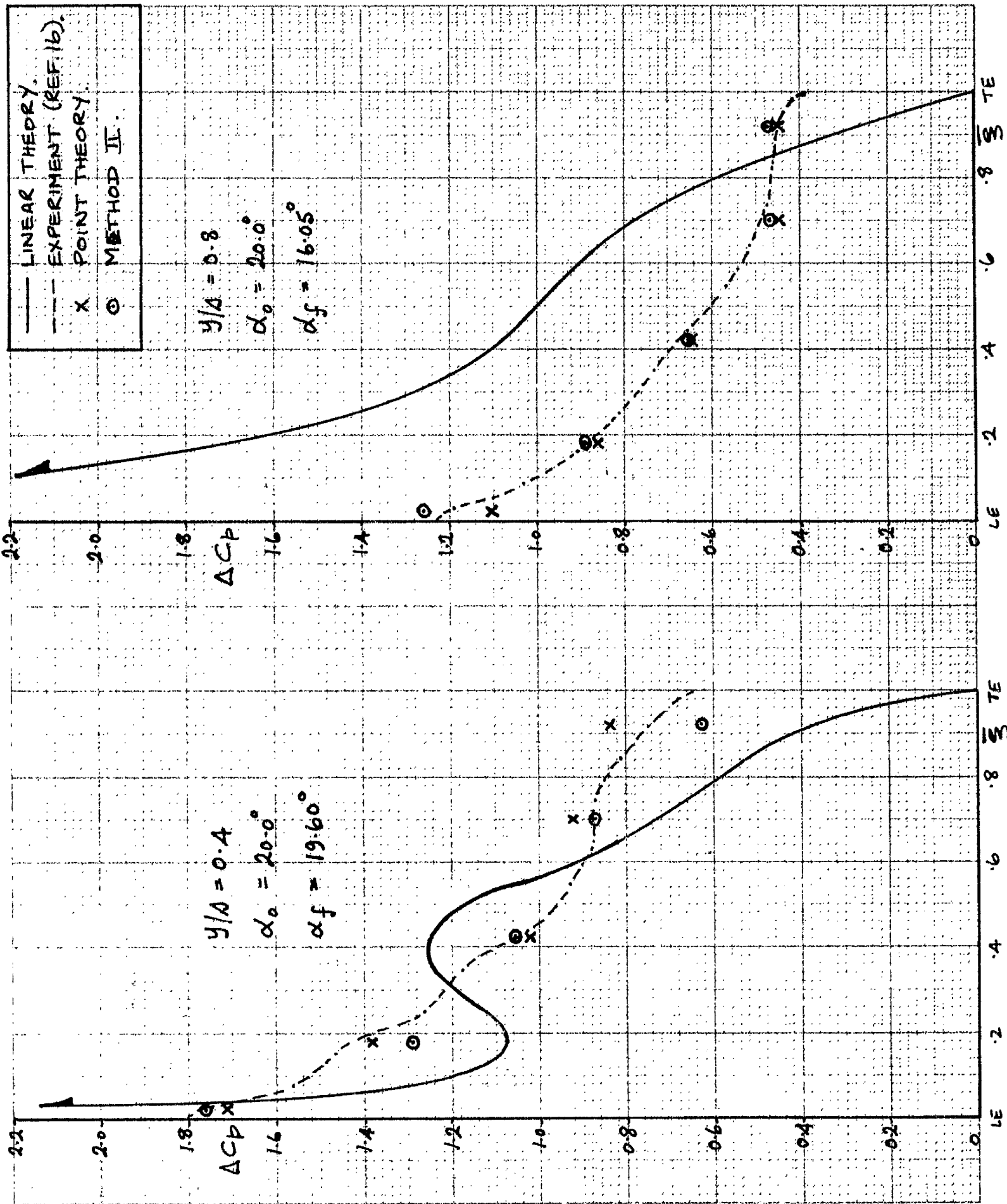


FIGURE 9C : - CUBIC WING MODIFIED PRESSURE DISTRIBUTION.
 $M = 0.94.$

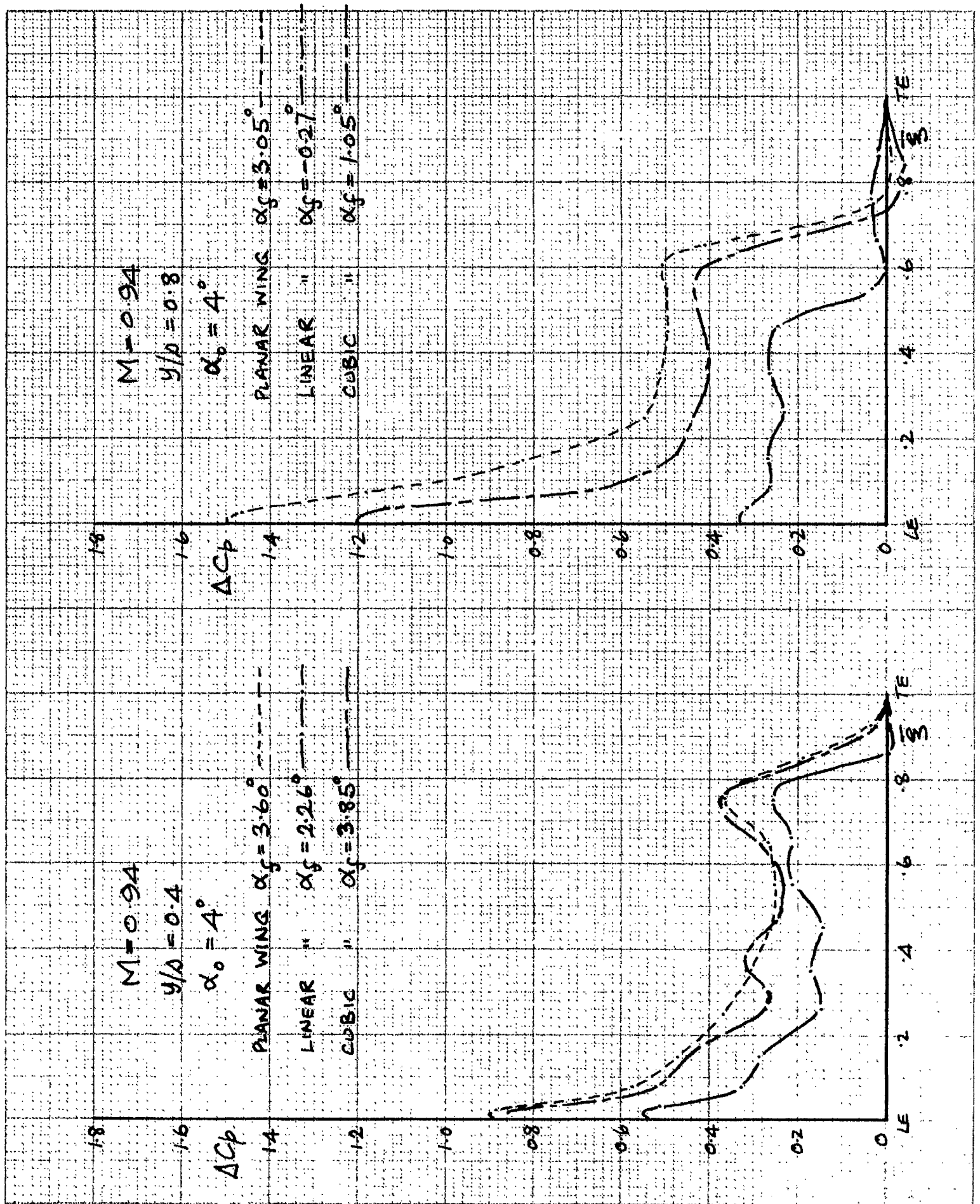


FIGURE 10:- PLANAR I, LINEAR AND CUBIC WING MEASURED PRESSURE DISTRIBUTIONS. $M = 0.94, \alpha_0 = 4^\circ$

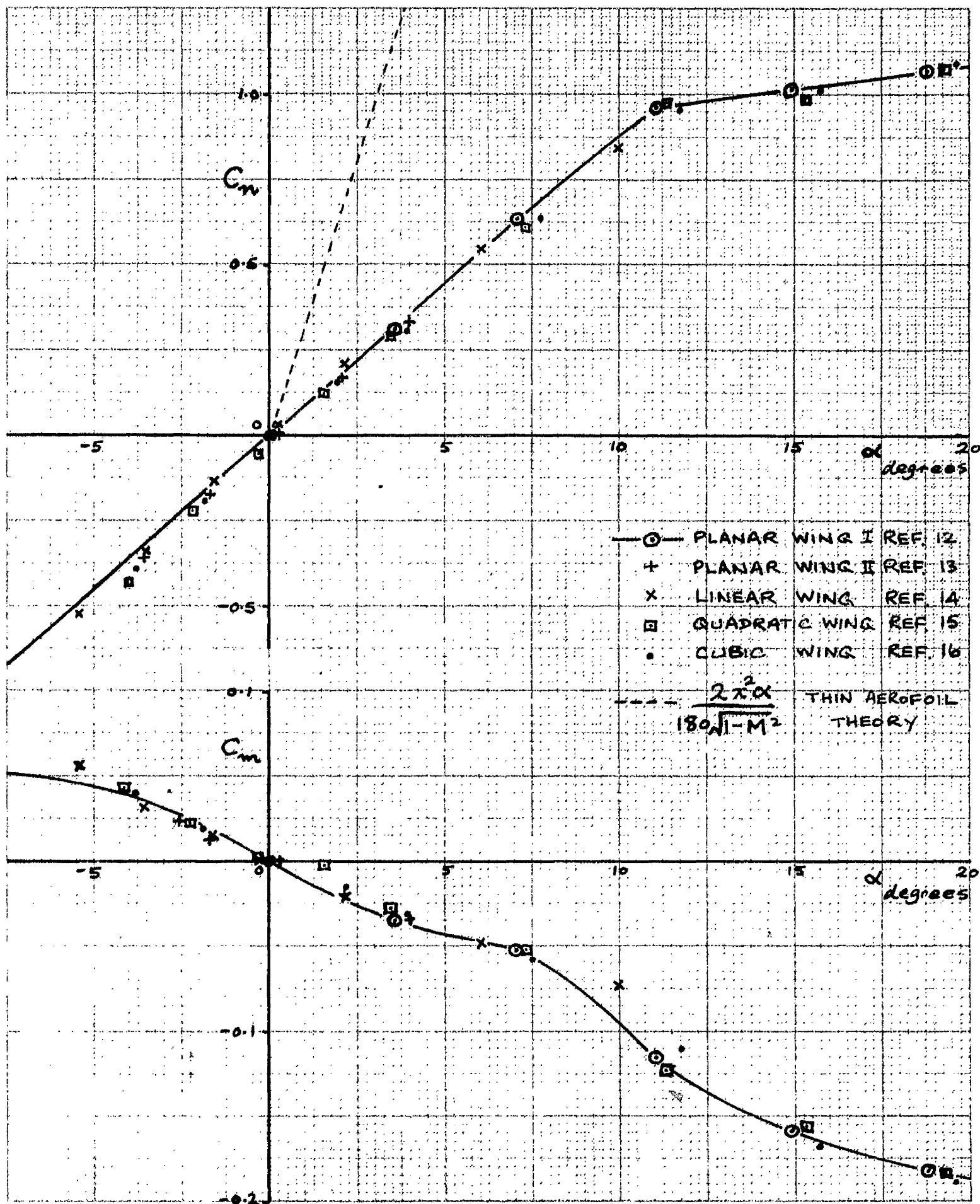


FIGURE 11 a:- LOCAL NORMAL-FORCE AND PITCHING MOMENT COEFFICIENTS. $M = 0.94$. $y/\Delta = 0.4$.

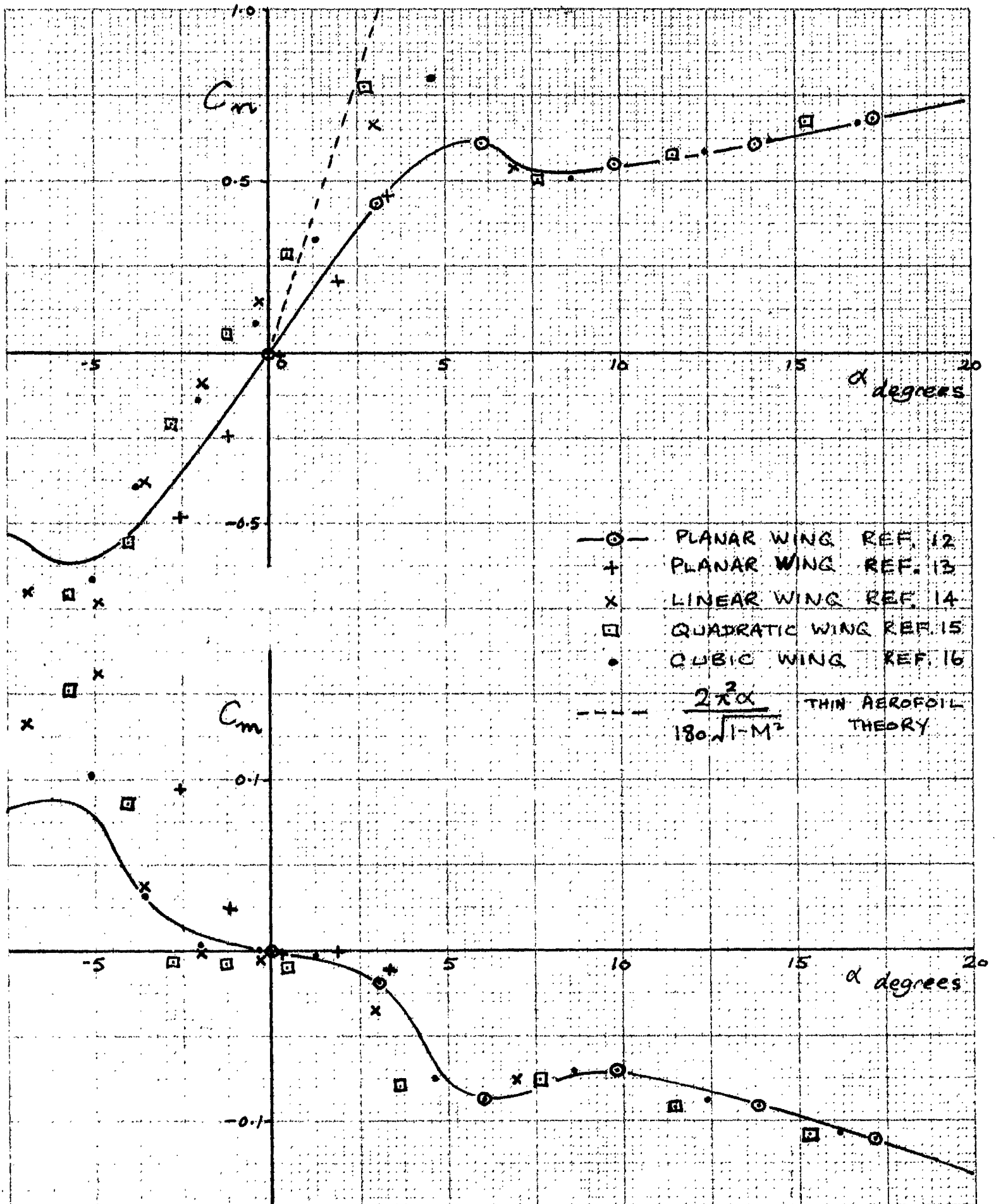


FIGURE 11b:- LOCAL NORMAL-FORCE AND PITCHING MOMENT COEFFICIENT. $M=0.94$. $y/b=0.8$.

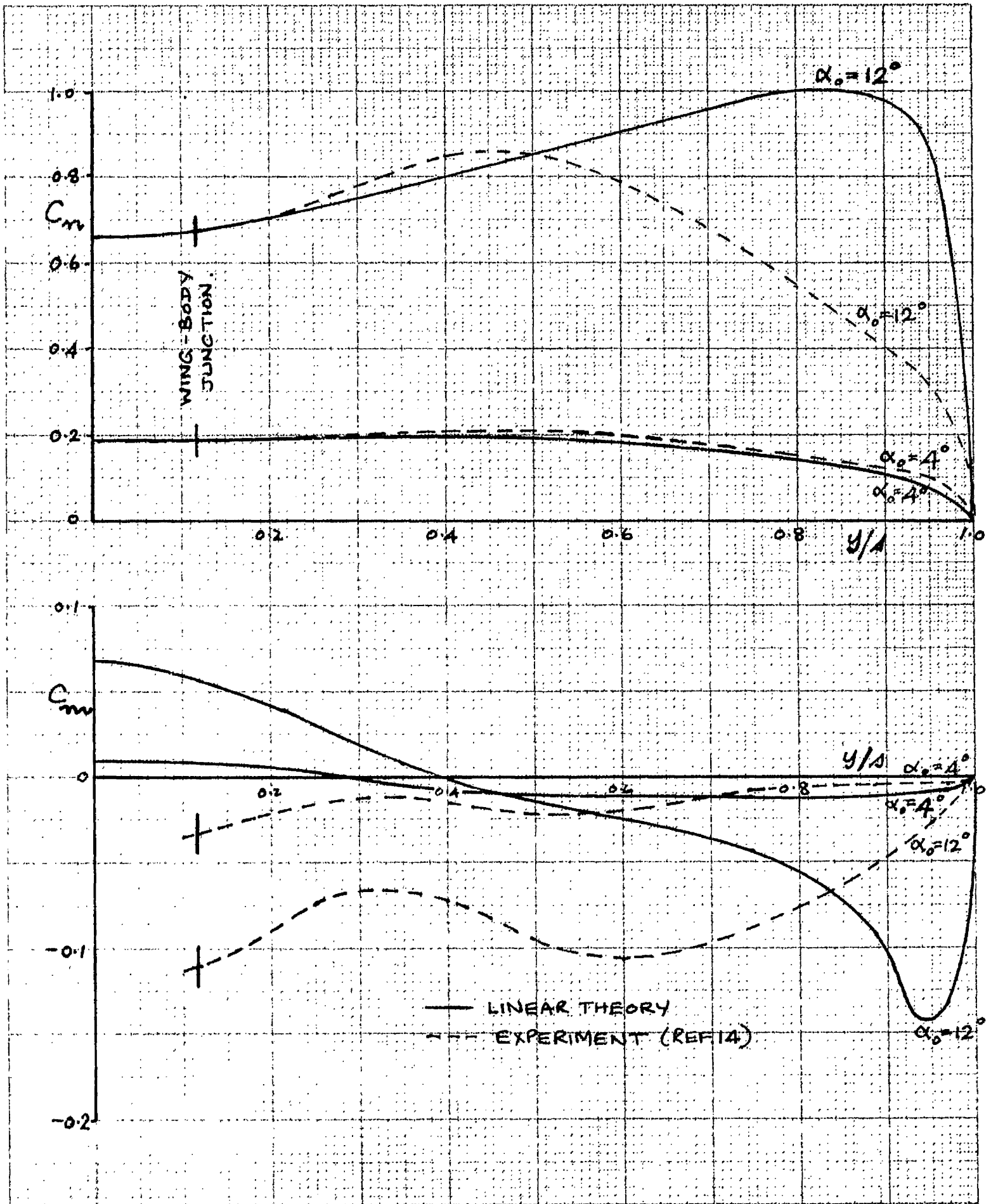


FIGURE 12: - COMPARISON OF THE THEORETICAL AND EXPERIMENTAL LIFT AND PITCHING MOMENT COEFFICIENTS (C_m AND C_m) WITH ~~MODIFIED THEORY~~ FOR LINEAR WING. $M=0.94$

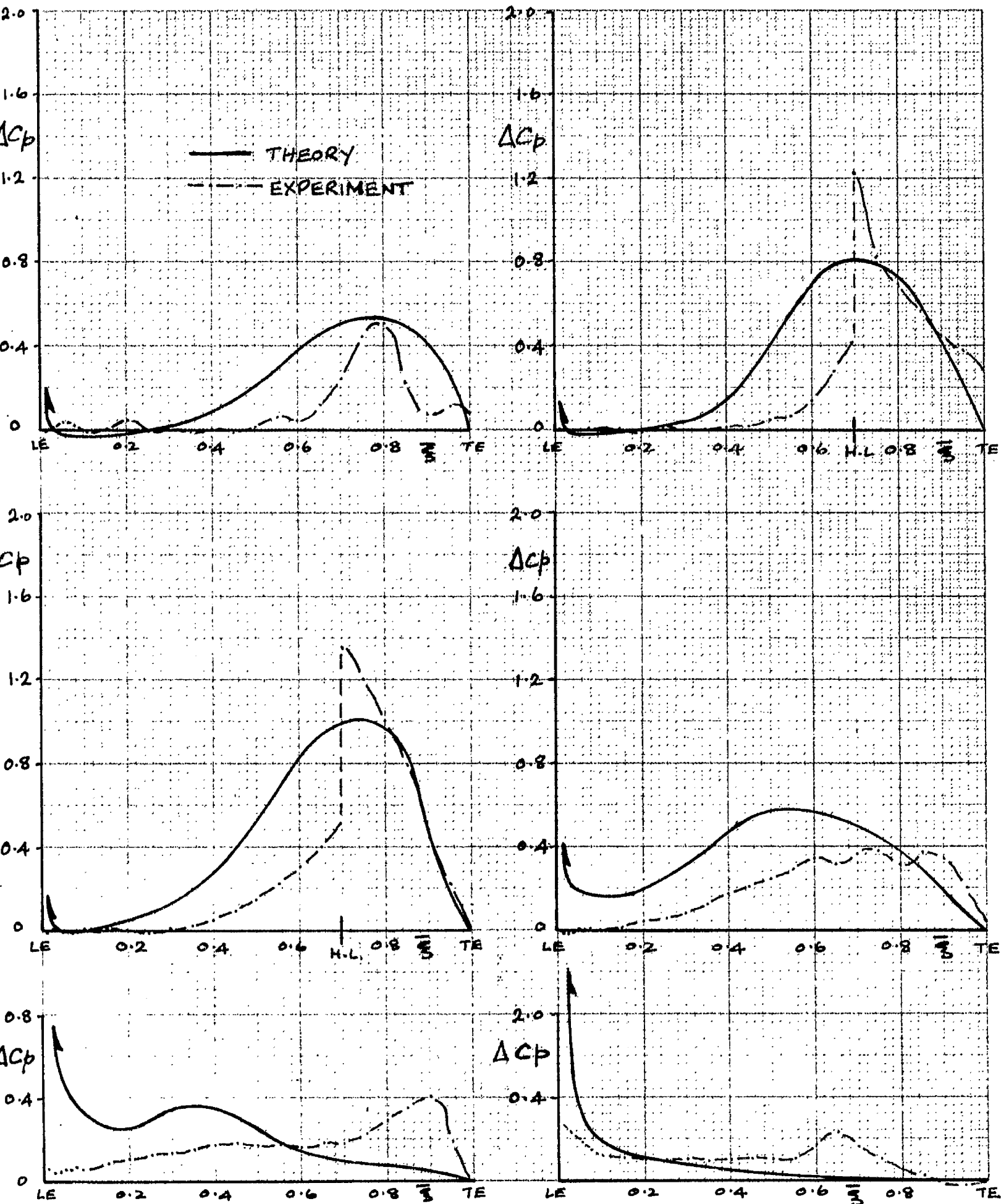


FIGURE 13 :- CONTROL SURFACE PRESSURE DISTRIBUTIONS. $M=0.94$
 CONTROL ANGLE $\delta=14.5^\circ$. $\alpha_0=0$

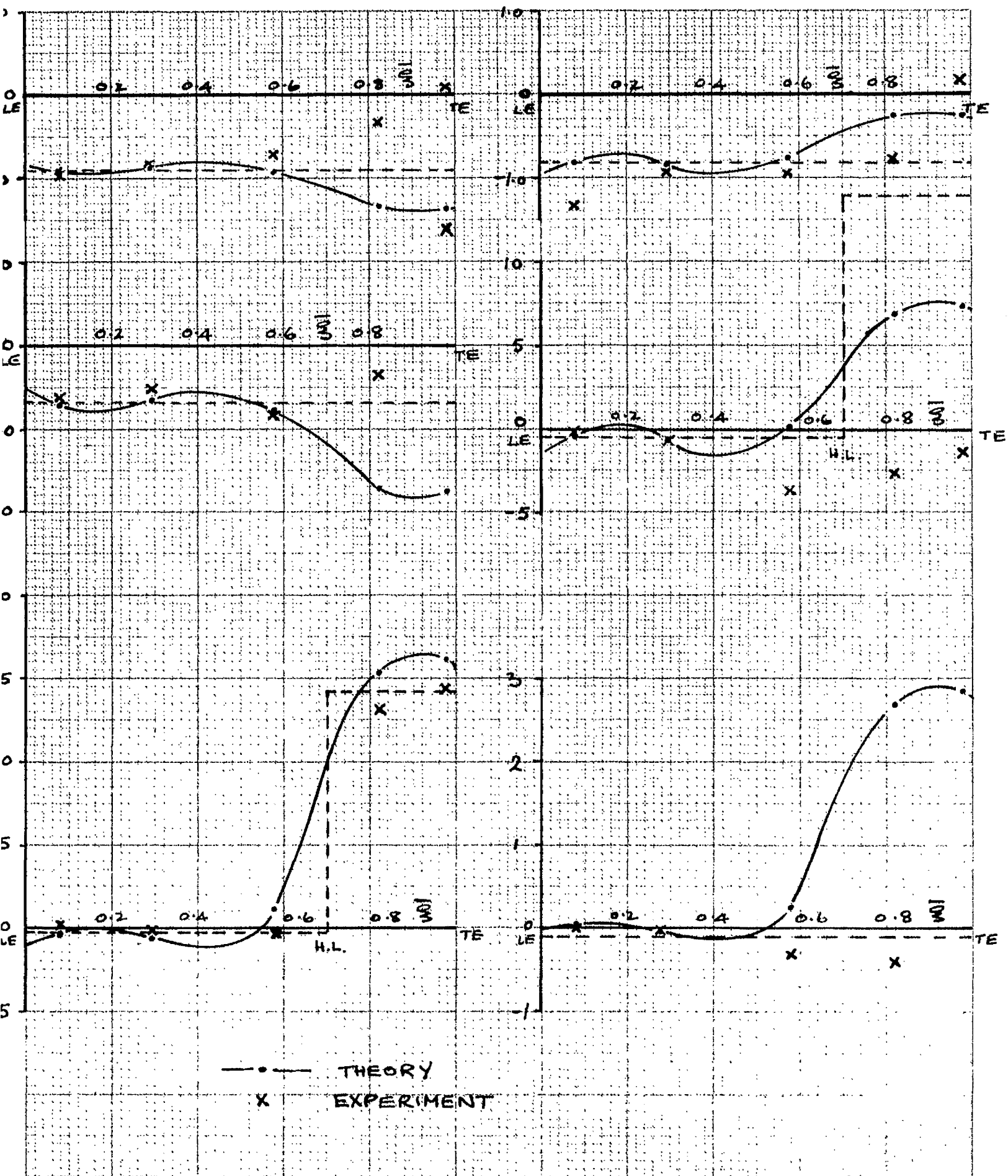


FIGURE 14:— EXPERIMENTAL AND THEORETICAL EQUIVALENT SLOPES.